

TITLE

In-situ determination of the mechanical properties of crawling or non-motile bacteria by Atomic Force Microscopy under physiological conditions without immobilization.

AUTHORS

Samia Dhahri¹, Michel Ramonda² and Christian Marlière^{1*}

AFFILIATIONS

1. Geosciences Montpellier, University Montpellier 2, UMR CNRS 5243, Montpellier, France
2. Centrale de Technologie en Micro et nanoélectronique, Laboratoire de Microscopie en Champ Proche, University Montpellier 2, Montpellier, France

* CORRESPONDING AUTHOR

Dr. Christian Marlière¹

Geosciences Montpellier, UMR 5243 CNRS, University Montpellier 2
Bat. 22 - C.C. 60- Place Eugène Bataillon, F-34095 Montpellier Cedex 5 - France
Phone: (+33) 670 532 190 / email: christian.marliere@um2.fr

ABSTRACT

We present a new, non-perturbative, easy-to-apply method for AFM imaging of living bacteria in their genuine physiological liquid environment. No immobilization protocol, neither chemical nor mechanical, was needed. For the first time, the native gliding (crawling) movements of gram-negative filamentous *Nostoc* cyanobacteria, along the surface and at speeds up to 200 nm/s, were studied by AFM. With the AFM working in a fast approach/retract mode, no limitation in neither spatial resolution nor imaging rate was detected. Gram positive and non-motile *Rhodococcus wratislaviensis* bacteria were studied as well. From the approach curves, Young modulus and turgor pressure were measured for both strains and for different gliding speeds. Young modulus is ranging from 20 to 105 MPa and turgor pressure from 40 to 310 kPa depending on the bacterium and the gliding speed. For *Nostoc*, spatially limited zones with higher values of stiffness were observed. The related spatial period is much higher than the mean length of nodules of *Nostoc*. This was explained by inhomogeneous mechanical activation of nodules in the cyanobacterium. We observed the presence of a soft extra cellular matrix (ECM) around the *Nostoc* bacterium. Both strains left a track

¹ Present address :

Institut des Sciences Moléculaires d'Orsay, ISMO CNRS, Université Paris Sud, Bât. 350, 91405 Orsay cedex, France

of polymeric slime with variable thicknesses. For *Rhodococcus*, it is equal to few hundreds of nanometers, likely to promote its adhesion to the sample. While gliding, the *Nostoc* secretes, behind it, a slime layer the thickness of it is in the nanometer range and increases with the gliding speed. This result reinforces the hypothesis of a propulsion mechanism based, for cyanobacteria, on ejection of slime.

These results open a large window on new studies of both dynamical phenomena of practical and fundamental interests such as the formation of conglomerates of bacteria (biofilms) and static properties of bacteria in real physiological conditions.

KEYWORDS

AFM; atomic force microscopy; bacteria; cyanobacteria; gliding movement; crawling movement; turgor pressure; elastic modulus; Young modulus; extra cellular matrix; slime; biofilms; *Anabaenopsis circularis*; *Rhodococcus wratislaviensis*.

INTRODUCTION

Atomic force microscopy (AFM) is a very powerful tool to get precious information about the nanoscale surface architecture of cells, the localization and interactions of their individual constituents with various internal and external agents. For instance, purified bacterial membranes have been imaged with very high resolution revealing the evolution of the organization of photosynthetic membranes in response to light [1]. Changes of cell surface structure were observed in physiological conditions during the germination of *Aspergillus fumigatus conidia* [2] at a resolution of a few nanometers. The nanomechanical properties of live cells have been mapped quantitatively using high rate dynamic AFM with a resolution in sub-10 nm range [3]. Recently very high-speed atomic force microscopy with nanometer resolution revealed the action of the antimicrobial peptide on individual *Escherichia coli* cells [4].

One important common aspect of all these reported results is that the employed method had to *immobilize* the cells firmly enough to enable them not to be swept out during the AFM scanning. The claimed aim was to withstand the lateral friction forces exerted by the tip during scanning without denaturing the cell interface and surface. As mentioned in many recent papers and reviews [5],[6],[7] that immobilization step has been considered as mandatory. In order to increase that adhesion of microorganisms, such as bacteria, to surfaces for imaging by AFM in liquid, many protocols have been proposed. One of the first used method requires the drying of the sample [8], therefore limiting drastically cell viability [9]. Furthermore re-immersion in the buffer medium was a challenging step. Many methods based on the use of various chemical ligands between the micro-organisms and the sample have been proposed such as polyphenolic proteins extracted from the marine mussel[10]. An another very common technique consists of pretreating the support with polycations, such as poly-L-lysine [11] or derivatives. However, the active groups used in covalent binding and the reagents used for cross-linking are known to affect cell viability by cross-linking the proteins on the cell surface [12] or may induce cell porosity [13]. Mechanical entrapment in aluminum oxide filters [14] or in isopore polycarbonate membrane s[15] were developed to avoid slow poisoning by chemical immobilizing and proved to be effective. Such entrapment methods are mainly suitable for imaging and force measurements of spherical cells. However bacteria may be in a state of mechanical stress far away from their standard living conditions. Furthermore this technique may impede the monitoring of active processes such as cell division. Other physical methods based on the trapping in soft gels as agar gel, gelatin layers [16] have been considered but these extracellular structures may lead to artifacts in AFM images. Recently, a method for the

assembly of living cells on specific areas of samples has been proposed. It consists in assembling the living cells within the patterns of microstructured, functionalized poly-dimethylsiloxane stamps using convective/capillary deposition [17].

Because of immobilization by glues or chemicals or by entrapment in membranes' pores, the cells are likely far away from their natural physiological conditions, a limiting factor for the biological relevance of such obtained results. Furthermore, by immobilization, one important aspect of many bacteria is overshadowed: Depending on the strain, bacteria may move inside the buffer medium by swimming or along limiting surfaces by gliding. In this last case bacteria used to form the so-called biofilms [18]: an association of extracellular polymeric substances (EPS) with structured, multicellular communities. Such biofilms are of very practical importance as they concern ubiquitous issues as in geophysical domain[19] and is prevalent in natural, industrial and hospital settings [20] etc. An important parameter in the formation of biofilms is the mobility of bacteria. Many gram-negative and gram-positive bacteria have been shown to possess surface layers and appendages (for instance type IV pili) useful for their motility [21][22][23]. However a large part of bacteria exhibits the ability to be motile along a surface without the aid of flagella. The *Nostocales* belong to this group of motile bacteria and contains most of the species of cyanobacteria capable of gliding [24][25]. Gliding is a form of cell movement that does not rely on any obvious external organ or change in cell shape and occurs only in the presence of a solid sample [26][27]. The gliding mechanism itself has been mainly studied using conventional optical microscopy by the evolution of a pre-deposited seedling root on an agar gel. However, due to its gelatinous cell walls, bacteria adhere strongly to the agar gel [27]. Optical observations require observing the gliding movement at very long times, typically a day or more. The first moments of gliding and consecutively its mechanism are thus unreachable [28]. Different hypotheses about the origin of the gliding in filamentous cyanobacteria have been proposed: it could be powered by a "slime jet" mechanism, in which the cells extrude a gel through pores surrounding each cell septum providing a propulsion force [29][30][31]. An alternative hypothesis is that the cells use contractive elements that produce undulations running over the surface inside the slime tube like an earthworm [32]. A recent study, done on immobilized bacteria (in dental wax), was based on the use of static AFM data [33] and scanning electron microscopy and revealed that arrays of parallel fibrils may be involved in the gliding mechanism. Recent observations were made by new ellipsometric optical microscopy technics on *Myxococcus xanthus* [34]. These authors observed that slime is

deposited at constant rate underneath the cell body slime. They suggested that this polymeric layer promotes the adhesion of the bacterium to the substrate without a real participation to the motility machinery.

Here we developed a new and simple method for AFM imaging of living bacteria in their standard (physiological) liquid environment without any immobilization step. Two examples of very different strains are presented. First a non-motile species (*Rhodococcus wratislaviensis*, IFP 2016, IFP Energies Nouvelles, Rueil-Malmaison, France, gram positive [35]) for which highly spatially resolved AFM images are obtained. Secondly, a filamentous cyanobacterium (*Anabaenopsis circularis*, PCC 6720, Institut Pasteur, Paris, France, gram negative) well known for its gliding movement on surfaces of glass slides was studied. With this last bacterial strain we were able to visualize for the first time the bacterium *during* its gliding movement on a glass slide by using AFM at a high acquisition rate (one image per minute and above) without limitation in spatial resolution. Different gliding speeds, from few tens to hundreds of nanometers per second, as obtained by cross-compared optical microscopy and AFM data, were studied. These results are a direct proof of the low impact of these breakthroughs AFM observations on the native behavior of the bacteria as the living character of the bacterium is verified thanks to its movement. No supplementary staining procedure for fluorescence studies was needed.

From high speed approach-retract curves, also called indentation curves, mechanical parameters as inner turgor pressure and Young modulus (linked to the surface elasticity of the bacterial membrane) were measured for bacteria naturally colonizing the sample's surface i.e. without the use of any perturbative immobilization steps. Furthermore these data were gathered in strictly physiological conditions for a large range of gliding speeds of the cells: from non-motile *Rhodococcus wratislaviensis* to few hundreds of nanometers per second for the gliding *Nostocs*. Thanks to this study we separate three major components in the bacterial entity: (1) the bacterium itself with a Young modulus ranging from 105MPa for gram positive *R. wratislaviensis* to 20MPa for gram negative *Nostoc* at low gliding speed; mean value of E_{Young} was shown to increase with gliding speed; our data revealed the presence of zones with high stiffness, the spatial periodicity of which is near by 20microns i.e. approximately one bacterial nodule over four; (2) the extracellular matrix (ECM) with E_{Young} in the range 4-15MPa depending on the gliding speed of *Nostoc*; for *R. wratislaviensis* no ECM was detected in the present operating conditions; and (3) a polymer excreted by the bacterium, the slime, to likely promote its adhesion to the sample's surface (*R. wratislaviensis*) or its gliding (*Nostoc*). In that last case our results suggest that both the thickness of the slime and the Young modulus increase

with the gliding speed, a different behavior of that observed with *Myxococcus xanthus* [34] for which slime is deposited at a constant rate independently of the gliding speed. We remark that for the zero or very low gliding speeds both bacterial types have similar slime values of E_{Young} (around few MPa). For *Nostoc*, our experiments showing the increase of the thickness of the slime layer with the gliding speed reinforces the hypothesis of Hoiczyk et al. [30] of propulsion by ejection of slime. We note too that the slime systematically has a lower value of stiffness and larger thickness at the high concavity side as for an increase of the friction coefficient to provoke the curved gliding.

RESULTS

We successively studied two categories of bacteria: first *Rhodococcus wratislaviensis* [35], a gram positive bacterium currently used for degradation of mixtures of hydrocarbons, known to be non-motile on the colonized surfaces and, second, *Nostoc* gram-negative bacteria able to glide on solid samples without the help of flagella or pili.

We first report results on *R. wratislaviensis*. Height images were taken in liquid phase (MM medium) by using QI mode (see Material and Methods section) and are plotted in figure 1 in 2D (figure 1.a) or in 3D (figure 1.b) in following conditions: 256 by 256 pixels, scan width 5 microns, acquisition time for one image around 10 minutes. The maximum applied force during the approach of the AFM tip was 10nN: Figure 2 shows typical approach curves on bacterium and on the glass slide. The mean indentation depth in bacterium is around 40 nanometers. In the 3D image very fine topographic details on bacteria membranes as small protuberances are better evidenced. It should be noted that the AFM image quality in liquid, moreover for non-immobilized bacteria, is unsurpassed [36,37]. The mean height of such bacteria is around 1 micron for a typical width of 1.2 micron. Two height profiles are plotted (figures 1.c and 1.d). In these, a shoulder is clearly visible at the right side of the main part of the bacteria and corresponds to a lower thickness (around 150nm) than on the central part of the bacterium (lateral expansion 450nm). These images are very stable in time as several acquisitions were done during two hours without any noticeable changes in conformation. The corresponding stiffness image is shown in figure 1.e. The two stiffness profiles along the two scan lines as defined in height data are plotted in figures 1.f and 1.g. It must be pointed out that these values of stiffness are effective ones as they result from the association of two linear springs in series [38], one being the AFM's cantilever and the other the bacterium envelope. The "glass slide" level corresponds to a

stiffness of 0.35 ± 0.01 N/m, the typical value of the stiffness of the working cantilever. This is very near from the value we obtained by standard determination based on thermal noise[39] : $k_c = 0.36 \pm 0.01$ N/m. This value is the maximum of the stiffness we can measure thanks to our AFM system as it works as a mechanical low-pass filter limited by the finite elasticity of the cantilever. This upper level is clearly evidenced by the light gray level in stiffness image. The effective stiffness of the bacterium has a value of around 0.23 to 0.25N/m. The shoulders at the right side of bacteria, as defined above, are characterized by an effective stiffness of around 0.11N/m. These three main levels of stiffness are more visible in the histogram plot of the stiffness values (figure 3). Peak number 1 (P1) corresponds to the glass sample (0.35N/m), P2 to the bacterium (0.23N/m), and P3 to the shoulder at the right of bacteria (0.12N/m). Please note that these effective stiffness values have been determined by using automatic peak detections (lorentzian shape assumed) through *OriginPro8.5* software (from *OriginLab*). That smaller value for effective stiffness (P3) is related to the presence of a polymeric layer, we will define it as *slime*, slightly besides the main part of the bacteria. The small protuberances on the membranes of *R. wratislaviensis* are related to dark grey spots in stiffness images, zones with lower stiffness. We also investigated *R. wratislaviensis* with a higher lateral resolution as it is shown in figure 4 where new data (256x256 pixels) with a scan size of 1 micron were taken. Minute details on the membrane of the bacterium as the presence of a slime layer nearby the bacterium are clearly evidenced. In the histogram data (Fig. 4.d) of the stiffness image (figure 4.c) three peaks are clearly visible and are positioned at stiffness values very similar to those previously determined: 0.35N/m (the glass slide contribution : upper and right corner of the image), 0.24N/m (bacterium's membrane) and 0.10N/m (slime). These results demonstrate that topographic and mechanical AFM data of high spatial resolution can be acquired by using our experimental protocol and set-up without the introduction of any external immobilizing step: only the natural adherence of the bacterium on the sample through the slime layer contributes to the feasibility of the acquisition of such AFM data: no parasite sweeping movements of bacterium during the AFM scan was detected.

In a second step cyanobacteria were studied. By means of optical microscope we first observed gliding movement of these filamentous *Nostoc* along the surface of the solid sample. Figure 5 is a typical example of such motility: the arrow indicates the successive positions of one of the nodule over time. Such motility was optically observed whatever the presence (see Fig. 5) or not (not shown) of the AFM tip and cantilever nearby or on the bacteria. One typical curve giving the variation of the X position (horizontal axis) of one of the *Nostoc* nodules when the AFM tip is fully retracted is plotted in figure 6.a. As well known, forward and backwards movements are observed. Same kind of

observations was done later when the AFM tip scanned the sample as in figure 5: the typical variation of X position is plotted (black line) in figure 6.b. The Y position of the AFM cantilever is plotted in lower parts of figures 6.b and 6.c. Optical images were taken every 4 seconds; AFM images were recorded every 35 seconds. During the acquisition of the AFM data the cantilever is systematically –whatever the relative orientation of the main axes of the cantilever and the filamentous bacterium- starting from the bottom-left corner of the image before imaging the first line parallel to the horizontal axis of the image. The second scan line starts from the left side of the image. The starting time of each AFM image is marked by a small vertical segment as indicated in figures 6.b and 6.c.

We will successively describe three typical sets of AFM data taken with the *Nostoc* cyanobacteria.

The first one is that already mentioned about the optical lateral displacement data. As indicated in figure 6.b and 6.c. five successive AFM images (64X64 pixels; $40.3\mu\text{m} \times 7.6\mu\text{m}$) were taken and are plotted in figure 7. In figure 7.6 an optical image at approximately the same magnification is shown for comparison. Figures 7.5 (AFM data) and 7.6 (optical data taken at the right side of the AFM investigated zone) remarkably revealed that same features are visible: nodules the mean length of which is around 5 microns are evidenced with two small vertical bumps in front and back positions. The *Nostoc* is clearly moving backwards (from right to left of the image) between images 1 and 2 (figure 7) before gliding in the opposite direction between images 2 to 5. In figure 7.3 a slight distortion in the structure of the nodules is visible in this AFM data: there is indeed a shift of the left extremity of the nodules towards the left side of the image when looking from the bottom to the top of the image (i.e. the vertical scan direction). This axial deformation across the width of the bacterium can thus be measured to $1.5\mu\text{m}$ from AFM data. As seen in figure 6.c the bacterium is accelerating –as determined by optical data- during the acquisition of AFM image number 3 (maximum absolute speed around 500nm/s). As the mean width of the bacterium is around 2 microns (see below) the related AFM vertical scanning time is estimated to 9 seconds. The resulting deformation is thus evaluated to 2 microns, very similar of the directly measured value. One important consequence of this consistency between AFM and optical data is that we observe the same movement along the whole chain of nodules. It means that hypothetic perturbations due to the AFM scanning are minimal. This conclusion is enforced when variation of position of the “head” of the *Nostoc* as measured by AFM is plotted with optical data: see stars (*) in figure 6.b. There is a remarkable agreement for the three first AFM images. A small discrepancy is visible for the next images: it is explained by the following reason. As, first, the head of the bacterium is near of the left border of the image and, second, the bacterium is accelerating in AFM image number 3, the nodule checked at the left side for

the variation of position of bacterium in time may not correspond to the head nodule of the bacterium: one another nodule passed away in front of AFM tip. Indeed the shift in bacterium displacement between AFM and optical data is approximately equal to 4 microns, very near to the typical value of a nodule length. The same kind of explanation may be advanced for the last AFM pictures as a second nodule passed through.

As already mentioned topographic and mechanical information are simultaneously acquired by AFM. Three examples are given in figures 8-10 where height and effective stiffness profiles are plotted either for different positions of the profile (along the vertical dashed line; figures 8 and 9) in a same AFM picture or at different positions of the bacterium on the sample (figure 10). From the topographic data the mean height and width of *Nostoc* are estimated to 2.2 μ m and 1.8 μ m respectively. In the stiffness profiles the level of the effective stiffness corresponding to the glass slide is well visible at both sides of these profiles. In figure 8, the mechanical profile over the bacterium is more complex as the central part has an effective stiffness of around 0.22N/m and edges around 0.06N/m, about one order of magnitude lower. Furthermore the value of stiffness at the border of the bacterium in the concavity of the chain of nodules is slightly lower than on the other side (60 \pm 5mN/m instead of 70 \pm 5mN/m). Same kinds of features are observed along the profile near the head of the gliding bacterium (figure 9). As before the stiffness at the border of the bacterium in its concavity is lower (70 \pm 5mN/m instead of 90 \pm 5mN/m). Another important feature we observe (figures 8 and 9) is the modulation of the effective stiffness along the longitudinal axis of the bacterium with a period we estimated to 20 μ m, the equivalent of roughly 4 nodules. The mean value of the effective stiffness for the bacterium as obtained from the histogram plot (figure 9.d) is equal to 90 \pm 5mN/m. In figure 10 related to a case where the curvature of the *Nostoc* is less pronounced, the dissymmetry for the stiffness values between both sides of the bacterium is small: 90 \pm 5mN/m in the concavity to be compared to 85 \pm 5mN/m on the other side.

By changing the color/gray scale in order to enhance minute details both in height (figure 11.c) and stiffness data (figure 11.d) ahead of the present position of the *Nostoc*, it is clearly visible that the bacterium left a trace during its former backwards and forwards movements. Profiles along the vertical dash line (figure 11.a-d) are plotted in figures 11.e and 11.f. A polymeric deposit with a typical height in the range of few nanometers and a mean stiffness of roughly 0.28N/m, as determined from histogram data (not shown), is clearly evidenced. The thickness of that slime is higher on both sides (around 6nm) than in its central part (\approx 3nm). Stiffness of lateral parts of the slime is lower (0.26 \pm 0.01N/m at the concave part of the track and 0.29 \pm 0.01N/m on the other side) than in its central part (0.30 \pm 0.01N/m). As the two sides of the slime track have the same height we can conclude that there is a slight

difference in the elastic properties of the slime between its both sides: stiffness is lower in the concavity. Because of the low value of the slime thickness, the influence of the underlying glass slide cannot be excluded: the values for stiffness are likely overestimated.

The second set of data about *Nostoc* bacteria is now presented. We optically observed too that, in this case too, the gliding of the *Nostoc* bacteria along the surface of the glass slide is parallel to the symmetry axis of these filamentous cyanobacteria. As above an optical estimation of the mean speed along the vertical axis of the image gave a value of $200 \pm 20 \text{ nm/s}$ (the bacterium is moving from the bottom to the top of the image). In figure 12.a-c are presented successive AFM images of the *Nostoc* bacterium: All these height images have been displayed in the same color scale (color range: $0.7 \mu\text{m}$). The setpoint value was set at 9.4 nN . Scanning time for one picture is 79s. The characteristic shape of connected elementary nodules with a mean length of around 4 microns is clearly visible in figures 12.a and 12.b. One remarkable feature must be pointed out: between the images 12.a and 12.b, a vertical (along the slow scan axis) shift of the main features is clearly evidenced (figure 12.a). In figure 12.d this spatial shift along the symmetry axis of the cyanobacterium is illustrated. The AFM data from picture 12.a is virtually up-shifted by $19.3 \pm 0.2 \mu\text{m}$ (white arrow) and superimposed over figure 12.b. The resulting image is shown in figure 12.d. The correlation between both images is good as main features of the *Nostoc* are well recognizable in two AFM pictures. It is thus possible to estimate the gliding speed: we get $245 \pm 25 \text{ nm/s}$, very near from the optical evaluation ($200 \pm 40 \text{ nm/s}$). On the third AFM picture (Figure 12.c) the bacterium is absent as it glided away from the AFM scanned zone. An estimation of the *minimum* gliding speed between images 12.b and 12.c gives a value of $260 \pm 25 \text{ nm/s}$. The passing-away of the *Nostoc* on the glass sample due to its gliding is well evidenced in stiffness images: stiffness values are plotted pixel by pixel in figure 13 (13.a and 13.b: bacterium is present; to compare with figures 12.a and 12.b; 13.c without bacterium). These data corroborate our observation made earlier: a thin layer of a material about twice softer than the cantilever has been left by the cyanobacterium on the glass during its gliding movement. Height and stiffness profiles on bacterium (along red line in figures 12.b and 13.b) and on the slime (along blue line in figures 12.b and 13.b) are plotted in figures 14.b and 14.c respectively. The slime thickness is around 20nm with a slightly higher value in the concavity of the bacterium curvature. Stiffness values for bacterium (figure 14.b2) and slime (figure 14.c2) are slightly smaller in the concavity. It should be noted that, contrary to what we measured with the first set of data on cyanobacteria (figures 7-11) stiffness at both sides of bacterium (figure 14.b.2) is very similar to that of the central part of bacterium (around 0.2 N/m). Mean values for the effective

stiffness for bacterium and slime can be well distinguished by comparing secondary peaks in histogram plots (see figure 15) corresponding to AFM data in figure 13.a and figure 13.c. We get $0.18\pm0.01\text{N/m}$ ($0.22\pm0.01\text{N/m}$) in case of bacterium (slime respectively).

A last sequence of data about *Nostoc* bacteria is presented (figures 16-17). The main direction of movement (first image: figure 16.a; second one: figure 16.b) of the bacterium (from top to bottom of AFM image) is opposite to slow scanning direction of AFM tip. From the AFM data the mean speed of the *Nostoc* bacterium is evaluated to $120\pm10\text{nm/s}$. The two consecutive stiffness images are separated by 137 seconds. Slime left by the bacterium in its former movement is clearly visible in figures 16.a and 16.b by the curved gray track. What we observe in these images is that the *Nostoc* is changing its direction of propagation by leaving its former track and going straight down the AFM image. Height (figure 16.c) and stiffness (figure 16.d) profiles along full (first AFM image: figure 16.a) and dashed lines (figure 16.b) have been plotted. Both sides of bacterium still reveal smaller values of stiffness: $50\pm5\text{mN/m}$; no dissymmetry between both sides is visible here. Profiles at the lower part of AFM images, where slime track and bacterium are spatially separated, are plotted in figure 17. The stiffness of the bacterium in its lower part reaches values as low as $30\pm5\text{mN/m}$ and does not present dissymmetry as observed in the former cases. This may be correlated to the straight movement of the *Nostoc*. As before, harder points are still present with a stiffness values around 0.2N/m . For this sequence stiffness of the slime track has a high value around 0.23N/m for a mean value of thickness of 8nm . As observed earlier, the thickness at the concavity side is slightly higher. The presence of two distinct levels for stiffness for bacterium and its slime is confirmed by histogram plot of stiffness data (figure 16.e): The peak at $0.25\pm0.01\text{N/m}$ has almost constant amplitude and corresponds to the slime zone as it does not change in area in AFM images during the movement of bacterium. Instead the peak at $0.07\pm0.01\text{N/m}$, a mean value over the whole length of the *Nostoc*, can be related to the bacterium as it increases in intensity when the *Nostoc* glides down the AFM scan zone. It must be emphasized that good reproducibility of our AFM measurements both for height and stiffness is clearly evidenced in figures 17.c and 17.d on slime signals, i.e. for the left part of the profiles.

DISCUSSION

Main points this study deals with can be summarized as follows:

As shown above, the method we develop for preparing the samples and AFM imaging allows us to observe two types of very different bacterial strains in their natural liquid media and on a standard sample (glass slide) in

excellent conditions. Gram positive and gram negative as well bacteria with very different types of shape and surface behavior were investigated.

Thanks to the absence of an immobilization step based on chemical or mechanical entrapment these bacteria were studied in purely native conditions without any external stress. We showed that natural gliding movement of the *Nostoc* cyanobacteria was preserved and detected by AFM in excellent conditions. In the case of non-motile bacteria (*R. wratislaviensis*) we obtained highly spatially resolved AFM images for standard scan times in native conditions. Details on their membrane were revealed by both topographic and mechanical stiffness data: for instance, small protuberances on the *R. wratislaviensis* membrane are observed in height images and correspond to zones with slightly lower stiffness. On height images and profiles (figure 1) low bumps with a typical thickness of 250nm and a lateral extension in the range of 450n were imaged besides the bacteria (on their right sides, see figure 1.a-b). These bumps are observed too in the stiffness images and are characterized by a low effective stiffness value of around 0.10N/m (see more details below). This external polymeric layer as defined by the stiffness value of around 0.10N/m is observed not only in the vicinity of the bacteria in contact with the sample but also at its interfaces with neighboring bacteria. We think this polymeric layer is likely involved in the adhesion of the bacterium to the glass slide and in the connections to neighboring bacteria, the early steps for the completion of a biofilm. This could be the trace deposited by the *R. wratislaviensis* in an initial slight migration along the surface followed by a self-immobilization step. The distance along which the cell slightly moves laterally before immobilizing could be tentatively estimated to 450nm, the lateral extension of this slime compound.

The study of cyanobacteria showed, for the first time, it was possible to make AFM images of high quality on a motile organism gliding over the surface of a glass slide at speed as high as 250nm/s. The characteristics of gliding movement of the *Nostoc* as deduced from both optical and AFM data are identical. Furthermore no correlation between the AFM tip and *Nostoc* movements was observed. These two last points enforce the conclusion that no major perturbation of its natural gliding movement is caused by the scan of the AFM tip above the cell. The bacterium is thus staying in its standard living state.

Stiffness profiles and histograms made from the whole stiffness images bring important and complementary information to height images. We were thus able to distinguish between two or three main components for the bacterial complex depending on the bacterial strain. In case of *R. wratislaviensis* we already mentioned the presence of a slime compound present around the bacteria characterized by a low effective stiffness of around 0.10N/m.

Comparatively the stiffness of the pure bacterial part is much higher: around 0.23N/m. Equivalent values were measured from stiffness histogram plots made on the whole AFM images. It can thus be deduced that the membrane of *R. wratislaviensis* bacterium is mechanically homogeneous. The slight variations of the local mechanical properties are connected to topographic features.

In case of motile bacteria we could wonder if classical indentation method by AFM is relevant. As a matter of fact in our AFM experiments the indentation approach lasts 1ms for a height variation of 500nm. As the relevant portion of the indentation curve is scanned in the range of 100nm, with a typical gliding speed of 200nm/s the bacterium advances of 40pm during the acquisition of one pixel in stiffness image. Consequently the bacterium can be considered as immobilized for every pixel of the image.

Contrary to *R. wratislaviensis*, the situation is more complex for the *Nostoc* cyanobacteria. In the stiffness histogram plots, only one peak (except that related to the cantilever) is detectable (figures 9.d, 15, 16.e) and corresponds to low values for the mean effective stiffness : around 0.09N/m for the first and last sequences we studied and around 0.18N/m for the sequence number 2. In these first two cases these low values for mean stiffness are related to a mean gliding speed of about 100nm/s. In the sequence number 2, higher value for mean stiffness corresponds to a gliding speed about twice higher (220nm/s). It must be noted that stiffness profiles perpendicularly to the axis of the filamentous bacterium (figures 8.d, 9.c, 10.d, 11.f, 14.b2, 14.c2, 16.d, 17.d) reveal a high heterogeneity: effective stiffness may reach 0.2N/m in the central part of the bacterium whatever the studied sequence. On the opposite, lateral parts of the bacteria have lower stiffness values down to around 0.05N/m for low gliding speed sequences and around 0.16N/m in the case of a mean gliding speed of 220nm/s. The distribution of stiffness along these profiles is more homogeneous in case of the fast bacterium (sequence 2). Large zones with low values of stiffness are observed (dark zones in figures 8.a, 9.a, 10.b, 11.b). Furthermore it must be remarked that the distribution, along the longitudinal axis of the *Nostoc*, of the zones with high stiffness (white zones in figures 8.a, 9.a, 10.b, 11.b) is not related to the spatial periodicity of the nodules: only few of them are in a state of high stiffness. The longitudinal position of these high stiffness regions along the chain of nodules relatively to the head of the *Nostoc* (figures 8.a and 10.b) is preserved during the gliding.

An important feature in case of *Nostoc* bacteria is that the gliding movement left a track of *slime* that can be directly observed on both height and stiffness data (see figures 11.e; 11.f; 14.c1; 14.c2; 17). From stiffness values reported in table 1, we note that the stiffness for the slime does not vary so much between the different sequences.

Its mean value is evaluated to an approximate value of 0.2N/m much higher than that of the ECM compound. This higher value of stiffness of the slime may be attributed to a partial contribution of glass sample through the thin slime layer causing an apparent hardening of the equivalent substrate. We observe a net increase of the slime thickness with the *Nostoc* gliding speed (figure 20). Figures 11.e and 17.c related to low gliding speeds show that the slime thickness is higher on both edges of the track left by the *Nostoc* in its gliding movement. This effect is not visible for high speed sequence probably because of an increased swelling of this thicker polymeric slime layer. As the ECM was also detected along the edges of the bacterium, the production of the slime could tentatively be related to the presence of the ECM along the bacterium. The higher value of stiffness for the slime left by the bacterium in its advance, when compared to that of the ECM, could be probably due to a temporal change of the properties of the polymeric deposit during the movement of the *Nostoc*, an aging effect of the initial polymer. When the gliding speed increases we note the presence of a *stiffer* ECM layer at the edges of the bacterium and the expulsion of a *thicker* slime layer. Production of ECM and slime could be connected.

From a careful look at stiffness profiles a questioning observation can be done. Stiffness values of the ECM are not symmetrically distributed along the two edges of the bacteria. According to our data lower values are located at the concave edge and that this effect is more pronounced for parts of the chain of nodules with a higher concavity (see figures 9.b and 14.b2 for high concavity zones instead of figures 16.d and 17.d for the opposite case). We note also that the stiffness of the slime is systematically lower on the side of high concavity as it can be seen for the three sequences in figures 11.f, 14.c2 and 17.d. Does the motility machinery of the cell excrete a thicker and softer compound at the edge of the highest concavity in order to increase friction coefficient and provoke the curved movement? New experiments are scheduled to answer this question.

Important mechanical parameters can be derived from the effective stiffness data. At first, by considering the AFM/tip mechanical system as the association of two linear springs in series [38], we are able to calculate the real stiffness of the bacterium, k_b , the ECM, k_{ECM} , and the slime, k_{slime} , instead of their effective stiffnesses. These data are reported in table 1: values for effective stiffness are in normal characters and stiffness for bacterium in italic ones. Getting relevant values of mechanical parameters of the bacterium from k_b is a hard task as the indentation stiffness of the bacterium wall is governed by several terms: these associated with stretching and bending of the cell wall, terms related to the surface tension and those directly related to the turgor pressure [38], the difference in pressures between the inner and the outer part of the bacterium as delimited by the cell membranes. In one recent

case [40], independent measurements of elastic modulus of the cell wall and turgor pressure of *E. coli* were done by comparing results from intact and bulging cells as obtained by using likely aggressive antibiotic agents (kanamycin and vancomycin). Most of the time, by applying some hypotheses [8,38] and referring to independent measurements of the Young modulus of biofilms (an association of bacteria and ECM), the stiffness data taken on the bacteria have been classically interpreted as a measurement of the turgor pressure.

From calculations of Boulbitch [41] and Arnoldi et al. [38] on the deformation of bacterial envelopes by an AFM tip for determination of the turgor pressure, Yao et al. [8] present a simple model to approximate turgor pressure based on tension dominated concept for the deformation of bacterial envelopes. It reduced the considerable mathematical complexity of the problem of turgor pressure calculation by elucidating some of the components that contribute to the overall deformation. The turgor pressure is then derived from the averaged slope (s) of the high force regime of the force spectrum in a similar manner to what has been done in this paper for all the so-called effective stiffness data (see figure 2). From s the bacterium stiffness, k_b , is obtained and, by applying equation (13) in reference [8], the turgor pressure is calculated. We used following parameters: R_b , the effective radius of the bacterium, equal $1.8\mu\text{m}$ and r_t , the mean tip radius, $r_t = 50\text{nm}$. As a first step we limit this study to data averaged over the whole bacterium as deduced from the histogram plots in order to compare these values for turgor pressure with data in literature. These scarce available data are indeed obtained from non-local investigations (with the recent exception [42]). A detailed study of the spatially repartition of the turgor pressure over the bacterium is under work. These mean values of the turgor pressures for the *Nostoc* and *R. wratislaviensis* bacteria in their growth media are reported in table 3. These experiments confirm the fact that turgor pressure is lower for gram-negative bacterium as *Nostoc*. They reveal that, for Gram negative *Nostoc* bacterium, the turgor pressure depends noticeably on the mean gliding speed: at low speeds (below 100nm/s) we got an averaged value of $50\pm10\text{kPa}$. It reaches a value of $174\pm30\text{kPa}$ in case of gliding speeds as high as 220nm/s .

Literature reveals that turgor pressure of gram-negative bacteria, immobilized by various ways for AFM measurements, depends on different factors as the ionic strength of the buffer or the presence or the absence of appendages [43]. In case of medium to high ionic strength (growth medium), values of turgor pressure range around $10\text{-}40\text{kPa}$ for *Pseudomonas aeruginosa* strain [7], *Shewanella putrefaciens* or *oneidensis* bacteria [44], *Escherichia coli* [40]. Instead turgor pressure measured in distilled water or any other medium with low ionic strength is as high as $85\text{-}150\text{kPa}$ as for instance in case of *Magnetospirillum gryphiswaldense* species [38] or *E. coli* [42], i.e., as

remarked in [8] one order of magnitude higher. Thus the values we measured for the *Nostoc* gram-negative bacteria are in the average of those available in literature. We can mention too that the value for turgor pressure we got for slow gliding *Nostoc* (around 50kPa) is very near from these reported in literature for immobilized bacteria.

Data for gram-positive bacteria are scarcer. Determination of turgor pressure in *Bacillus-subtilis* was done in its growth medium and gave a value of 1.9 MPa [45]. For *Enterococcus hirae* [8] in distilled water turgor pressure was measured in the range 400-600kPa that could be extrapolated to values around 50kPa in growth medium. The value we measured for *R. wratislaviensis*, 307±20kPa, is intermediate between these two min-max values given by the literature. It must be emphasized that the stiffness (equivalent to turgor pressure as explained above) is much more homogeneous all over the *R. wratislaviensis* bacterium when compared with the *Nostoc*.

Independently of the measurement of the turgor pressure, the Young modulus which characterizes the elasticity of bacterial envelope can be determined from the curve giving the variation of the AFM applied force, at the low-force side, on the sample versus its indentation. This curve (figures 18.b) is obtained from the plots of the applied force during the approach of the AFM tip to the glass slide and the studied bacterium (figures 18.a): From the difference between this hard surface line and the observed deflection over the bacterium the indentation of the cell is calculated. The force versus indentation curve can be analyzed through theoretical models for quantitative information on sample elasticity. In order to get an estimate of the Young modulus of the different components of and around the bacterium we classically used the Hertz model [46]

$$F = \frac{2E \tan \alpha}{\pi(1-\nu^2)} \delta^2$$

with the Poisson coefficient, ν , equal to 0.5 and a semi-top angle, α , of the AFM tip we took equal to 35°.

Typical force versus piezo displacement curves for glass slide and for the different components of the bacterium are plotted in figures 18.a, 19.a. The related force versus indentation curves and the best fits by using Hertz model are plotted in figures 18.b and 19.b. Resulting values for the Young modulus are shown in table 3. In the case of *Nostoc* the so-called *bacterium* Young modulus only concerns the stiffest parts of the bacterium as the softest part have mechanical properties very similar to these of the surrounding ECM. It must be noted that the values for the Young modulus of the different components of the *Nostoc* do not vary with the studied sequence in the limit of experimental uncertainties.

Literature reveals that, even if studies are rather sparse, the value of elastic modulus of biofilms varies greatly, depending on the method used to measure it and the way the samples are prepared and studied [18]. Values as low as 7kPa were reported [47] for the Young modulus of the biofilms of *Pseudomonas aeruginosa* at the interface of an agar surface and humid air. Typical values for the elasticity of the bacteria are in the range 10-50MPa [40,48–50]. One recent study [42] gives a value of the Young modulus around 1MPa for the gram negative *E. coli* for in a 1 mM KNO_3 electrolyte. To our knowledge the results for Young modulus as presented in this paper are the first ones for living bacteria in physiological conditions. Furthermore we get values for Young modulus for the different components related to the bacteria: the bacterium itself, the slime and the ECM in case of the gliding *Nostoc*. We first confirm that the Young modulus is higher for gram positive *Rhodococcus* than for the gram negative *Nostoc* as it is observed in literature, almost one order of magnitude in case of low-speed cyanobacterium. It is currently explained by the fact the membrane wall is much thicker for Gram-positive bacteria than for Gram-negative. In case of *Nostoc*, values of E_{young} for ECM and slime slightly increase with the gliding speed. This tendency is also observed for the hard parts of the bacterium. For the non-motile *Rhodococcus* and for the *Nostoc* gliding at low speed as well, the slime has much lower Young modulus values than those related to the respective bulky parts of the bacteria. As slime thickness for *Rhodococcus* has a high value (250nm) there is no indentation of the underlying glass slide and, consequently, the measured E_{young} value, around 4MPa, properly characterizes the compressive modulus of this slime. Instead, for *Nostoc*, the slime thickness is much lower (lower than 20nm) and the Young modulus is very likely over-evaluated. We guess that for *Nostoc* in low speed regime a more realistic value for E_{young} could be in the range of few hundreds of kPa. For the *Nostoc* we observe that the E_{young} for slime is higher when the gliding speed increases. The Young modulus of the slime left by the cyanobacterium is indeed multiplied by a factor of almost 20 between the slow and fast gliding regimes. The mode of propulsion of the *Nostoc* bacterium may vary with the bacterium speed as we observe that the turgor pressure, the Young moduli of both the bacterium and slime and the thickness of the slime layer are modified.

Our observation, in case of *Nostoc*, of an increase of the thickness of the slime with the gliding speed is a point of importance. It indeed may reveal important information about the mechanisms of gliding of living organisms. For instance Hoiczyk and Baumeister [30] concluded from their optical and electron microscopy observations that the extrusion of slime comes from junctional pore complexes in the cell wall. They correlated the rate of slime extrusion with the speed of movement of the cyanobacterial filaments (*Phormidium uncinatum* and *Anabaena variabilis*) and

concluded that gliding movements are caused directly by the secretion of slime. A similar conclusion was drawn by Yu et al. [51] from the study of *Myxococcus xanthus* in the case of type A motile gliding as it was observed the extrusion of the slime from the rear pole of the cell. It can be anticipated [34] that the drag force to move the bacterium would increase linearly with velocity and thus the thickness of the slime should increase with the gliding speed. These authors studied *Myxococcus xanthus* deposited on a specially treated sample with the help of an optical microscope using an enhanced contrast technics based on ellipsometry. They revealed a clear correlation between the amount of slime deposit and the time spent by a cell at a given position suggesting that slime is deposited at constant rate underneath the cell body [34]. In case of *Nostoc*, as presented in this paper (figure 20), we instead observe a net increase of the slime thickness with the *Nostoc* gliding speed. An alternate explanation based on a spurious dependence of the slime thickness with residence time of the bacterium at one place of the sample can be very likely ruled out: a correlation between the measured speed and the real (and unknown) residence time seems to be unlikely as we observed such a behavior for different bacteria with probable very different history in terms of reverse movements. As a consequence the gliding process for the *Nostoc* is likely directly related to the extrusion process of the slime as mentioned in [30]. Our study also reveals that the nature of polymer as characterized by its Young modulus is depending on the gliding speed. In the low speed regime, E_{young} for *Nostoc* is small, very likely in the range of few hundreds of kPa. We already noted that this last value is roughly of the same order of magnitude compared to that measured with the non-motile *R. wrativialiensis*. We could wonder whether the variation of mechanical properties and thickness (in the range of tens of nanometers for motile cells, up to few hundreds of nm with *r. wrativialiensis*) of the excreted slime with the gliding speed could come from a common mechanism for bacteria able to glide or not.

One important improvement of our method when compared to optical microscopy often used in literature is that the slime can be mechanically characterized at an unprecedented low spatial scale. Figure 11, as an example, reveals interesting features along direction perpendicular to the cyanobacterium axis. Slime thickness is higher on both sides but stiffness was systematically observed to be lower at the most concave side of the bacterium or its track. A spurious effect on these relative values due to a partial influence of the underlying sample can be excluded as similar thicknesses of slime have clearly distinct values for stiffness as it can be seen along profile in figure 11.f. This lateral effect is clearly visible too with the ECM as in figure 9.c. for low gliding speeds and is still evidenced in case of high speeds (figure 14.b2) even in this more difficult conditions for AFM imaging. This effect may be responsible of the

curved propagation of the filamentous cyanobacterium as the friction at the centripetal side of the bacterium is increased when plunging in a thicker and more gelatinous layer of polymer.

We observed that the distribution of these zones of high stiffness along the longitudinal axis of the *Nostoc* is not connected to the spatial periodicity of the nodules: The *Nostoc* bacterium presents zones of high stiffness much more distant, around 20 microns (see figure 9) than the centers of nodules (mean length of a nodule approximates 6 microns). These observations could be explained by at least the following scenarios: (i) large zones recovered by such a thick layer of soft polymer (ECM) that the indentation only reveal the mechanical properties of this only ECM independently of the underlying substrate i.e. bacterium or glass slide; (ii) the *Nostoc* is moving as a caterpillar. The *Nostoc* would retract its body from the sample from place to place, leading to a disruption in mechanical contact with the glass slide and consequently causing a resulting vanishing of stiffness; (iii) a mechanical wave with an alternation of high and low stiffness zones running through the filamentous bacterium during its gliding. However as we did not measure noticeable variations of height along the nodules the two first hypotheses might be ruled out. Further investigations are in progress.

Unlike all available and used experimental ways of investigation, we dispose of a unique method for the detection of both topographic features and mechanical characteristics (stiffness, turgor pressure and Young modulus) at the sub-micrometer scale for both in-plane and height directions with alive organisms in physiological conditions. Unlike all available methods, detection of polymeric deposits is independent of their optical properties including very low or no optical contrast with surrounding tissues or sample. Electron microscopy offers an unprecedented lateral resolution but without real quantization of roughness and needs mandatory and drastic conditions of preparation of biological samples such as fixation procedures etc. Thus optical microscopy remains a standard method to observe living microorganisms but high resolution imaging is only possible with minimum specimen processing which are very often perturbative for the biological samples. Live imaging approaches have used optical fluorescence microscopy with specific stains to localize specific components in the studied cells and/or increase spatial resolution. The problem is still more complex with the study of extra-cellular polymer surrounding or excreted by organisms as the optical contrast in case of visible light is often very low. In differential interference contrast (DIC) and phase-microscopy, contrast enhancement of a transparent and unstained specimen is possible but such techniques are unfortunately unable to visualize sub-micrometric details of living cells and are quite perturbative. Recently a new technics was developed to specifically study the ECM and slime [34]. It was based on the enhancement of optical

contrast by the use of specially designed substrate coatings in which multiple reflections and interferences cause high contrast sensitivity to thin deposits. However in order to promote the adhesion of the studied *Myxococcus xanthus* a thin layer of chitosan and fibronectic was deposited on the glass-like substrate. The bacteria were thus in experimental conditions far from their physiological ones as disturbing external agent, chitosan [52] for instance, was used. By comparing the observation made with such a method and that from fluorescent-staining experiments these authors obtained interesting results on the *Myxococcus xanthus* system: (i) no slime deposition emanating from the ends of the bacterium was detected; (ii) slime seems to be distributed all over the cell envelope; (iii) that slime is deposited at a constant rate below the cell body whatever its speed. The authors suggest that the bacterium advances by a kind of pushing action of motility machinery by a “paste-release” mechanism greatly facilitated by the excretion of slime on the sample with variable adhesion properties. For *Nostoc* our experiments showed that the thickness of the slime layer is increasing with the gliding speed reinforcing the hypothesis of Hoiczyk et al [30] of propulsion by ejection of slime.

CONCLUSIONS

In summary, we presented a new, non-perturbative, easy-to-apply method for imaging living bacteria by AFM in their genuine liquid environment and in true *in-vivo* conditions, avoiding an immobilization step unanimously described as essential. This study was feasible thanks to a new AFM mode based on a very well controlled extend/approach curves made pixel by pixel and at a high speed. This mode strongly minimized the lateral interactions between the cantilever and the biological organism. We studied gram-positive, non-motile *R. wratislaviensis* strains and gram-negative, gliding *Nostoc* cyanobacteria.

On both bacterial strains height images of high quality were obtained by AFM in liquid. In particular we were able to follow the natural gliding movements of the *Nostoc* cyanobacteria both with AFM and optical imaging, directly proving the living state of the organisms during the AFM investigation and its very low impact on the biological state of the *Nostoc*. Our study revealed that AFM imaging is thus possible on moving living species with speeds as high as few hundreds nanometers per second. The AFM images of gliding cyanobacteria were acquired at a high AFM acquisition rate, typically one AFM frame per minute or higher, without limitation on spatial resolution. These breakthrough AFM observations strongly minimized perturbations on living cell when compared to common

procedures based on mechanical entrapment or chemical immobilization. For example, chemical stress due to immobilizing substances may induce cell porosity [13].

The mechanical properties of these two strains were studied at sub-micrometric scale and values for bacterial stiffness, Young modulus or turgor pressure were obtained. These data revealed the presence of three main components on and around the bacteria: (i) the bacterium itself with a Young modulus ranging from 20 to 105MPa and turgor pressure from 40 to 310kPa depending on the bacterium and its gliding speed ; (ii) a thin layer of polymeric slime left by the bacterium during its gliding movement or to promote its adhesion on the surface of the glass sample with Young modulus as low as few MPa and below for low speed moving bacteria; (iii) an extra cellular matrix (ECM) mainly present around the *Nostoc* bacterium. For *Nostoc* our experiments showed that the thickness of the slime layer is increasing with the gliding speed reinforcing the hypothesis of Hoiczyk et al. [30] of propulsion by ejection of slime. An important conclusion of this study is that excellent imaging quality can be obtained by AFM in liquid without the need of an artificial immobilization step of the bacteria on the sample. This opens a wide window on new studies based on the dynamics of living cells in purely controlled physiological conditions: motility of bacteria, formation of biofilms, influence of light on moving properties of cyanobacteria, effects of antibiotics on bacterial membranes and biofilm etc.

MATERIAL AND METHODS

Bacterial preparation

The cyanobacterial strains used in this work were *Nostoc* strain, PCC 6720 (formerly *Anabaenopsis circularis*) and were purchased from the Institut Pasteur Collection (CIP, Paris, France). Cyanobacteria are photoautotrophic gram-negative prokaryotes. These strains were grown in autoclaved standard BG11 liquid medium prepared from 50x concentrated cyanobacteria BG-11 freshwater solution (Sigma-Aldrich) and 18.2 MΩ.cm purified water (Milli-Q water purification system, EMD Millipore Corporation., Billerica, MA, USA). Before AFM experiments, cultures were incubated at 25°C at a constant incident flux of white light half the day in a dedicated chamber and were in contact with external air through anti-contamination filter. Bacteria were transplanted in fresh medium regularly.

The other studied strain is *Rhodococcus wratislaviensis*, capable of degrading multiple petroleum compounds in solution in aqueous effluents and registered at the Collection Nationale de Cultures de Microorganismes (CNCM), Paris, France under number CNCM I-4088 (provided by IFPEN). Stock cultures were kept frozen at -80 °C in 20% glycerol (v/v). The culture medium used was a vitamin-supplemented mineral medium (MM). After inoculation (10%), the adequate carbon source was added, and the cultures were incubated at 30°C with constant agitation. Cultures were grown in flasks closed with a cap equipped with an internal Teflon septum to avoid any loss of substrate either by volatilization or by adsorption. The headspace volume was sufficient to prevent any O₂ limitation during growth. Growth was followed by measuring the Optical Density at a wavelength of 660nm. Before AFM experiments, cultures were incubated at 25°C in a dedicated chamber and were in contact with external air through anti-contamination filter. Bacteria were transplanted in fresh medium regularly.

Sample preparation

The sample used for the AFM experiments was standard glass slide for optical microscopy. In a first step it was cleaned by sonication in a diluted solution of detergent (pH around 9) for 15 minutes before being carefully rinsed with high purity water (Milli-Q). Drying was done below the flux of a pure inert gas.

The bacterial suspension was vortexed then sonicated during three minutes in gentle conditions in order to get, in the final step, a surface density of bacteria of around 100 bacteria per mm². Few hundreds of microliters were then deposited on the glass slide. The excess of solution was then aspirated by a micropipette and the glass slide was further left in surrounding atmosphere for few minutes before being rinsed with the solution of BG 11. This sample was then placed under the combined optical/AFM microscope for liquid imaging in BG11 medium (liquid volume of

few hundreds of microliters). During AFM experiments, bacteria in liquid medium were in direct contact with atmosphere. AFM measurements were made in the two hours after inoculation of the glass plate.

Optical and AFM imaging

Atomic force microscopy (AFM) studies were carried out at a temperature of $27\pm1^{\circ}\text{C}$ using a Nanowizard III (JPK Instruments AG, Berlin, Germany). Experiments were operated in liquid (BG11 medium), using Quantitative Imaging® (QI) mode. The main characteristics of that mode is to measure a real and complete force distance curve at every pixel of the image, minimizing the lateral forces applied by the apex of the cantilever on the studied object. The pixel-by-pixel extend/retract curves were done at a constant speed of typically $500\ \mu\text{m}/\text{s}$ on a total extension of $500\mu\text{m}$. An additional retract length of 100nm was added before going to the next pixel. Typical images were done on the basis of a surface scanning by 128 by 128 pixels. The distance between two successive pixels along the sample surface is usually different along slow scanning axis (vertical in the reported AFM pictures) and fast scanning axis (horizontal) of the images. We used standard beam AFM probes (PPP-CONT^{PT}, Nanosensors, Neuchatel, Switzerland) with a nominal value of stiffness of $0.36\pm0.01\text{N}/\text{m}$, as measured by thermal noise[39], and a tip height of about 15 microns. The cantilever is recovered by a standard 25 nm thick double layer of chromium and platinum-iridium alloy on both sides. The maximum applied force was in the range of 10nN . All the presented AFM images are raw data (without any post-treatment as flattening etc). We checked that no noticeable contamination of the APEX of the tip was detectable. The AFM head is working on a commercial inverted microscope (Axio Observer.Z1, Carl Zeiss, Göttingen, Germany). During all the presented experiments the sample was illuminated by a LED illuminating system (white light) operating in transmission mode. Optical images were taken through a LD "Plan-Neofluar" 40x/NA0.6 objective (Carl Zeiss, Göttingen, Germany) by a standard color camera. Image analyzing was made through custom computing codes developed with Matlab R2011, The MathWorks Company, Natick, MA, USA.

ACKNOWLEDGEMENTS

The authors would like to thank A. Hermsdoerfer and T. Henze (JPK Instruments AG, Berlin, Germany) for fruitful discussions. Dr. R. de Wit, Ecologie des Systèmes Marins Côtiers, UMR 5119, University Montpellier 2, France, and Dr. O. Brunel, Hydrosciences Montpellier, UMR 5569, University Montpellier 2, France are gratefully acknowledged for helpful discussions. A. Desoeuvre gave us an efficient technical help. The authors are very grateful to IFP Energies Nouvelles, Rueil-Malmaison, France (Dr. Françoise Fayolle-Guichard and Yves Benoit) for the free disposal of *Rhodococcus wratislaviensis*, IFP 2016 strain, through Dr. Marie-Christine Dictor and Jean-Christophe Gourry, BRGM, Orléans, France. This work is funded by the Agence Nationale de la Recherche (ANR, Paris, France) through the program ECOTECH_2011 (project BIOPHY N° ANR-10-ECOT-014-05).

| | | | | Bacterium | ECM | Slime | |
|---------------------------|-----------------|---------------------|-----------------|---------------------------|--------------------------|-----------------|-------------------------|
| Type of Bacterium | Sequence number | Gliding speed (m/s) | Figure numbers | Stiffness (N/m) | Stiffness (N/m) | Stiffness (N/m) | Thickness (nm) |
| | | | | Mean value from histogram | Stiffest points | | |
| <i>Nostoc</i> | #1 | 80 | 8; 9; 10; 11 | 0.09 / 0.12 | 0.18-0.22 / 0.36-0.57 | 0.07 / 0.09 | 0.26-0.30 / 0.94-1.8 |
| | #2 | 220 | 14; 15; | 0.18 / 0.36 | 0.23 / 0.64 | 0.16 / 0.29 | 0.21 / 0.50 |
| | #3 | 120 | 16; 17 | 0.07 / 0.09 | 0.2 / 0.45 | 0.03 / 0.04 | 0.21 / 0.50 |
| <i>R. wratislaviensis</i> | | 0 | 3; 4 | 0.23 / 0.64 | 0.24 / 0.72 | - | 0.12 / 0.18 |
| | | | | | | | 250 |

Table 1

Values of effective stiffness and component stiffness (in italics) for the different studied bacteria and their different components.

| Type of Bacterium | Sequence number | Gliding speed (m/s) | Figure numbers | Turgor Pressure (kPa) |
|---------------------------|-----------------|---------------------|----------------|-----------------------|
| <i>Nostoc</i> | #1 | 80 | 8; 9; 10; 11 | 58 |
| | #2 | 220 | 14; 15; | 174 |
| | #3 | 120 | 16; 17 | 42 |
| <i>R. wratislaviensis</i> | | 0 | 3; 4 | 307 |

Table 2

Turgor pressure for the studied bacteria at different gliding speeds

| Type of Bacterium | | | Young modulus (MPa) |
|---------------------------|-----------|------------|------------------------|
| <i>Nostoc</i> | | | |
| <i>Nostoc</i> | Bacterium | Low speed | 20 ±3 |
| | | High speed | 63 ±5 |
| | ECM | Low speed | 4 ±2 |
| | | High speed | 15 ±3 |
| | Slime | Low speed | 1.1 ±1.0 |
| | | High speed | 20 ±3 |
| <i>R. wratislaviensis</i> | | | |
| <i>R. wratislaviensis</i> | Bacterium | | 104 ±5 |
| | Slime | | 4.3 ±.5 |

Table 3

Young modulus for the studied bacteria at different gliding speeds

REFERENCES

1. Scheuring S (2005) Chromatic Adaptation of Photosynthetic Membranes. *Science* 309: 484–487. doi:10.1126/science.1110879.
2. Dague E, Alsteens D, Latgé JP, Dufrêne YF (2008) High-resolution cell surface dynamics of germinating *Aspergillus fumigatus* conidia. *Biophysical journal* 94: 656–660.
3. Raman A, Trigueros S, Cartagena A, Stevenson APZ, Susilo M, et al. (2011) Mapping nanomechanical properties of live cells using multi-harmonic atomic force microscopy. *Nature Nanotechnology* 6: 809–814. doi:10.1038/nnano.2011.186.
4. Fantner GE, Barbero RJ, Gray DS, Belcher AM (2010) Kinetics of antimicrobial peptide activity measured on individual bacterial cells using high-speed atomic force microscopy. *Nature Nanotechnology* 5: 280–285. doi:10.1038/nnano.2010.29.
5. Dorobantu LS, Gray MR (2010) Application of atomic force microscopy in bacterial research. *Scanning* 32: 74–96. doi:10.1002/sca.20177.
6. Dupres V, Alsteens D, Andre G, Dufrêne YF (2010) Microbial nanoscopy: a closer look at microbial cell surfaces. *Trends in Microbiology* 18: 397–405. doi:10.1016/j.tim.2010.06.004.
7. Webb HK, Truong VK, Hasan J, Crawford RJ, Ivanova EP (2011) Physico-mechanical characterisation of cells using atomic force microscopy — Current research and methodologies. *Journal of Microbiological Methods* 86: 131–139. doi:10.1016/j.mimet.2011.05.021.
8. Yao X, Walter J, Burke S, Stewart S, Jericho M, et al. (2002) Atomic force microscopy and theoretical considerations of surface properties and turgor pressures of bacteria. *Colloid Surf B-Biointerfaces* 23: 213–230. doi:10.1016/S0927-7765(01)00249-1.
9. Mendez-Vilas A, Diaz J, Donoso MG, Gallardo-Moreno AM, Gonzalez-Martin ML (2006) Ultrastructural and physico-chemical heterogeneities of yeast surfaces revealed by mapping lateral-friction and normal-adhesion forces using an atomic force microscope. *Antonie Van Leeuwenhoek* 89: 495–509. doi:10.1007/s10482-005-9048-4.
10. Meyer R, Zhou X, Tang L, Arpanaei A, Kingshott P, et al. (2010) Immobilisation of living bacteria for AFM imaging under physiological conditions. *Ultramicroscopy* 110: 1349–1357. doi:10.1016/j.ultramic.2010.06.010.
11. Schaer-Zammaretti P, Ubbink J (2003) Imaging of lactic acid bacteria with AFM—elasticity and adhesion maps and their relationship to biological and structural data. *Ultramicroscopy* 97: 199–208. doi:10.1016/S0304-3991(03)00044-5.
12. Kailas L, Ratcliffe EC, Hayhurst EJ, Walker MG, Foster SJ, et al. (2009) Immobilizing live bacteria for AFM imaging of cellular processes. *Ultramicroscopy* 109: 775–780. doi:10.1016/j.ultramic.2009.01.012.
13. Colville K, Tompkins N, Rutenberg AD, Jericho MH (2010) Effects of Poly-lysine Substrates on Attached *Escherichia coli* Bacteria. *Langmuir* 26: 2639–2644. doi:10.1021/la902826n.
14. Kasas S, Ikai A (1995) A method for anchoring round shaped cells for atomic force microscope imaging. *Biophysical Journal* 68: 1678–1680. doi:10.1016/S0006-3495(95)80344-9.
15. Dufrêne Y (2001) Application of atomic force microscopy to microbial surfaces: from reconstituted cell surface layers to living cells. *Micron* 32: 153–165. doi:10.1016/S0968-4328(99)00106-7.
16. Doktycz M, Sullivan C, Hoyt P, Pelletier D, Wu S, et al. (2003) AFM imaging of bacteria in liquid media immobilized on gelatin coated mica surfaces. *Ultramicroscopy* 97: 209–216. doi:10.1016/S0304-3991(03)00045-7.
17. Dague E, Jauvert E, Laplatine L, Viallet B, Thibault C, et al. (2011) Assembly of live micro-organisms on microstructured PDMS stamps by convective/capillary deposition for AFM bio-experiments. *Nanotechnology* 22: 395102.
18. Flemming H-C (2011) The perfect slime. *Colloids and Surfaces B: Biointerfaces* 86: 251–259. doi:10.1016/j.colsurfb.2011.04.025.
19. Galvez ME, Beyssac O, Benzerara K, Bernard S, Menguy N, et al. (2012) Morphological preservation of carbonaceous plant fossils in blueschist metamorphic rocks from New Zealand. *Geobiology* 10: 118–129. doi:10.1111/j.1472-4669.2011.00316.x.
20. Bruneel O, Volant A, Gallien S, Chaumande B, Casiot C, et al. (2011) Characterization of the Active Bacterial Community Involved in Natural Attenuation Processes in Arsenic-Rich Creek Sediments. *Microb Ecol* 61: 793–810. doi:10.1007/s00248-011-9808-9.
21. Henrichsen J (1972) Bacterial surface translocation: a survey and a classification. *Bacteriol Rev* 36: 478–503.
22. Busscher HJ, Weerkamp AH (1987) Specific and non-specific interactions in bacterial adhesion to solid substrata. *FEMS Microbiology Letters* 46: 165–173. doi:10.1016/0378-1097(87)90062-0.

23. Vadillo-Rodriguez V, Busscher H, Norde W, de_Vries J, van_der_Mei H (2003) On relations between microscopic and macroscopic physicochemical properties of bacterial cell surfaces: An AFM study on *Streptococcus mitis* strains. *Langmuir* 19: 2372–2377. doi:10.1021/la020658l.
24. Youderian P (1998) Bacterial motility: Secretory secrets of gliding bacteria. *Curr Biol* 8: R408–R411. doi:10.1016/S0960-9822(98)70264-7.
25. Adams D, Ashworth D, Nelmes B (1999) Fibrillar array in the cell wall of a gliding filamentous cyanobacterium. *J Bacteriol* 181: 884–892.
26. McBride M (2001) Bacterial gliding motility: Multiple mechanisms for cell movement over surfaces. *Annu Rev Microbiol* 55: 49–75. doi:10.1146/annurev.micro.55.1.49.
27. Reichenbach H (1981) Taxonomy of the gliding bacteria. *Annu Rev Microbiol* 35: 339–364. doi:10.1146/annurev.mi.35.100181.002011.
28. Hanada Y, Sugioka K, Shihira-Ishikawa I, Kawano H, Miyawaki A, et al. (2011) 3D microfluidic chips with integrated functional microelements fabricated by a femtosecond laser for studying the gliding mechanism of cyanobacteria. *Lab Chip* 11: 2109–2115. doi:10.1039/C1LC20101H.
29. Hoiczyk E (2000) Gliding motility in cyanobacteria: observations and possible explanations. *Arch Microbiol* 174: 11–17. doi:10.1007/s002030000187.
30. Hoiczyk E, Baumeister W (1998) The junctional pore complex, a prokaryotic secretion organelle, is the molecular motor underlying gliding motility in cyanobacteria. *Curr Biol* 8: 1161–1168. doi:10.1016/S0960-9822(07)00487-3.
31. Hoiczyk E, Baumeister W (1995) Envelope structure of four gliding filamentous cyanobacteria. *J Bacteriol* 177: 2387–2395.
32. Tamulonis C, Postma M, Kaandorp J (2011) Modeling Filamentous Cyanobacteria Reveals the Advantages of Long and Fast Trichomes for Optimizing Light Exposure. *PLoS One* 6. doi:10.1371/journal.pone.0022084.
33. Read N, Connell S, Adams DG (2007) Nanoscale Visualization of a Fibrillar Array in the Cell Wall of Filamentous Cyanobacteria and Its Implications for Gliding Motility. *J Bacteriol* 189: 7361–7366. doi:10.1128/JB.00706-07.
34. Ducret A, Valignat M-P, Mouhamar F, Mignot T, Theodoly O (2012) Wet-surface–enhanced ellipsometric contrast microscopy identifies slime as a major adhesion factor during bacterial surface motility. *PNAS* 109: 10036–10041. doi:10.1073/pnas.1120979109.
35. Auffret M, Labbé D, Thouand G, Greer CW, Fayolle-Guichard F (2009) Degradation of a Mixture of Hydrocarbons, Gasoline, and Diesel Oil Additives by *Rhodococcus aetherivorans* and *Rhodococcus wratislaviensis*. *Appl Environ Microbiol* 75: 7774–7782. doi:10.1128/AEM.01117-09.
36. Bolshakova A., Kiselyova O., Filonov A., Frolova OY, Lyubchenko Y., et al. (2001) Comparative studies of bacteria with an atomic force microscopy operating in different modes. *Ultramicroscopy* 86: 121–128. doi:10.1016/S0304-3991(00)00075-9.
37. Zhavnerko G, Nikolaevich Poleschuyk N (2012) Mycobacterium under AFM tip: Advantages of polyelectrolyte modified substrate. *International Journal of Mycobacteriology* 1: 53–56. doi:10.1016/j.ijmyco.2012.01.009.
38. Arnoldi M, Fritz M, Bäuerlein E, Radmacher M, Sackmann E, et al. (2000) Bacterial turgor pressure can be measured by atomic force microscopy. *Physical Review E* 62: 1034.
39. Levy R, Maaloum M (2002) Measuring the spring constant of atomic force microscope cantilevers: thermal fluctuations and other methods. *Nanotechnology* 13: 33–37. doi:10.1088/0957-4484/13/1/307.
40. Deng Y, Sun M, Shaevitz JW (2011) Direct measurement of cell wall stress stiffening and turgor pressure in live bacterial cells. *Physical Review Letters* 107: 158101–1_4.
41. Boulbitch AA (1998) Deflection of a cell membrane under application of a local force. *Phys Rev E* 57: 2123–2128. doi:10.1103/PhysRevE.57.2123.
42. Polyakov P, Soussen C, Duan J, Duval JFL, Brie D, et al. (2011) Automated Force Volume Image Processing for Biological Samples. *PLoS One* 6. doi:10.1371/journal.pone.0018887.
43. Francius G, Polyakov P, Merlin J, Abe Y, Ghigo J-M, et al. (2011) Bacterial Surface Appendages Strongly Impact Nanomechanical and Electrokinetic Properties of *Escherichia coli* Cells Subjected to Osmotic Stress. *PLoS ONE* 6: e20066.
44. Gaboriaud F, Gee ML, Strugnell R, Duval JFL (2008) Coupled electrostatic, hydrodynamic, and mechanical properties of bacterial interfaces in aqueous media. *Langmuir* 24: 10988–10995. doi:10.1021/la800258n.
45. Whatmore AM, Reed RH (1990) Determination of turgor pressure in *Bacillus subtilis*: a possible role for K⁺ in turgor regulation. *J Gen Microbiol* 136: 2521–2526. doi:10.1099/00221287-136-12-2521.

46. Boulbitch A (2000) Deformation of the envelope of a spherical Gram-negative bacterium during the atomic force microscopic measurements. *J Electron Microsc* (Tokyo) 49: 459–462.
47. Korstgens V, Flemming H, Wingender J, Borchard W (2001) Uniaxial compression measurement device for investigation of the mechanical stability of biofilms. *J Microbiol Methods* 46: 9–17. doi:10.1016/S0167-7012(01)00248-2.
48. Yao X, Jericho M, Pink D, Beveridge T (1999) Thickness and Elasticity of Gram-Negative Murein Sacculi Measured by Atomic Force Microscopy. *J Bacteriol* 181: 6865–6875.
49. Thwaites J, Mendelson N (1989) Mechanical properties of peptidoglycan as determined from bacterial thread. *Int J Biol Macromol* 11: 201–206. doi:10.1016/0141-8130(89)90069-X.
50. Mendelson N, Thwaites J (1989) Cell-wall mechanical-properties as measured with bacterial thread made from *bacillus-subtilis*. *J Bacteriol* 171: 1055–1062.
51. Yu R, Kaiser D (2007) Gliding motility and polarized slime secretion. *Mol Microbiol* 63: 454–467. doi:10.1111/j.1365-2958.2006.05536.x.
52. Fernandes JC, Eaton P, Gomes AM, Pintado ME, Xavier Malcata F (2009) Study of the antibacterial effects of chitosans on *Bacillus cereus* (and its spores) by atomic force microscopy imaging and nanoindentation. *Ultramicroscopy* 109: 854–860. doi:10.1016/j.ultramic.2009.03.015.

FIGURE CAPTIONS

Figure 1

AFM height (a-b) and stiffness (e) images of *Rhodococcus wratislaviensis* in their physiological medium. (Height color scale: 2 μ m; stiffness grey scale 0.4N/m: scan size 5 μ m \times 5 μ m). Height (c-d) and stiffness (f-g) profiles along dashed lines in figures (a) or (e) are plotted.

Figure 2

AFM approach curves in liquid are plotted for the substrate (glass slide) and the bacterium (*Rhodococcus wratislaviensis*).

Figure 3

Stiffness histogram related to AFM stiffness image (figure 1.e) is presented.

Figure 4

AFM height (a-b) and stiffness (c) images of *Rhodococcus wratislaviensis* in their physiological medium are presented. These images are taken at zone delimited by the white square in figure 1 (Height color scale: 1 μ m; stiffness grey scale 0.4N/m; scan size 1 μ m \times 1 μ m). Stiffness histogram related to AFM stiffness image (figure 1.c) is presented in figure d.

Figure 5:

Optical snapshots of the gliding of *Nostoc* bacterium along the glass slide are shown. The scale is given by the black line (10 microns). The bacterium is moving from the right to the left of the images as indicated by the displacement of the landmark (arrow) between the two images ($\Delta t=12$ s). Width of the images (along X axis) is equal to 78 microns.

Figure 6:

Figures 6.a-b: The displacements of the *Nostoc* along the X axis, as determined from optical microscopy (as in figure 5), is plotted (full line) versus time during its gliding movement on the surface of the glass slide for two independent bacteria.

In figure 6.b the data are related to the reported sequence number 1 as explained in main text. The movement of the AFM cantilever is plotted versus time (black triangles; the line is a guide for the eye): every triangle corresponds to a measured position. The beginning of a new AFM image is marked by the small vertical segment; its number is labeled in the squared box. The positions of the bacterium as determined from AFM images (see figure 7) are marked by the stars (*).

In figure 6-c (upper curve with left triangles) gliding speed of *Nostoc* related to position data in figure 6.b is plotted versus time.

Figure 7

Successive AFM height (1-5) images of *Nostoc* in their physiological medium are plotted. Time interval between two consecutive images is equal to 35 seconds (Height color scale: 3 μm ; scan size: 40.3 $\mu\text{m} \times 7.6\mu\text{m}$). For comparison an optical image acquired during this AFM sequence was numerically treated to get the same magnification as in AFM images (1-5).

Figure 8

AFM height (a) and stiffness (b) images of *Nostoc* in their physiological medium are presented. They correspond to image 7.5: height color scale: 3 μm ; stiffness grey scale 0.4N/m; scan size 40.3 $\mu\text{m} \times 7.6\mu\text{m}$. Stiffness profile (d) along dashed line in figure (a) is plotted.

Figure 9

AFM height (a) and stiffness (b) images of *Nostoc* in their physiological medium are presented. They correspond to image 7.5: height color scale: 3 μm ; stiffness grey scale 0.4N/m; scan size 40.3 $\mu\text{m} \times 7.6\mu\text{m}$. Height (c) and stiffness (d) profiles along dashed lines in figures (a) or (b) are plotted. Stiffness histogram related to AFM stiffness image (figure 9.a) is presented in figure d.

Figure 10

AFM height (a) and stiffness (b) images of *Nostoc* in their physiological medium are presented. They correspond to image 7.3: height color scale: 3 μm ; stiffness grey scale 0.4N/m; scan size 40.3 $\mu\text{m} \times 7.6\mu\text{m}$. Stiffness profile (d) along dashed line in figure (a) is plotted.

Figure 11

AFM height (a, c) and stiffness (b-d) images of *Nostoc* in their physiological medium are presented. They correspond to image 7.3: scan size 40.3 $\mu\text{m} \times 7.6\mu\text{m}$; height color scales: 3 μm (a) / 50nm (c); stiffness grey scales: 0.4N/m (b) / 0.1N/m (d). Height (e) and stiffness (f) profiles along dashed line in figures (a-b) are plotted.

Figure 12

- Figure 12.a-c: Three AFM images of the gliding of *Nostoc* bacterium along the glass slide. In figure 2.c. the bacteria glided away from the AFM scan zone. Common Z scale: 0.7 μm (for the black/white color range. Scan size: 40 $\mu\text{m} \times 15\mu\text{m}$).
- Figure 12.d: Visualization of the vertical gliding movement (along the slow scan axis) of the *Nostoc*. It is done by the superposition (figure 12.d) of the image of the bacteria as determined in figure 12.b (bacterium at the right side of image 12.d) with that measured 79s earlier (figure 12.a) and vertically shifted along the white arrow (shift length: 19.3 \pm 0.2 microns). For reasons of clarity a lateral shift between the native figures 12.a and 12.b has been done.

Figure 13

Nostoc AFM stiffness images are presented. They correspond to the three equivalent height images in figure 12.a-c. (Z gray scale: 0.5N/m).

Figure 14

AFM height (_0, _1) and stiffness (_2) profiles of *Nostoc* bacterium (b_) along red line in images 12.b and 13.b and excreted slime (c_) along blue line in images 12.c and 13.c are plotted.

Figure 15

Stiffness histograms related to *Nostoc* AFM stiffness images in figure 13.a (dots) and figure 13.c (crosses) are presented.

Figure 16

a; b : two successive AFM stiffness images of *Nostoc* are presented: scan size 20 μm x20 μm ; stiffness grey scale: 0.4N/m. Time interval is equal to 137 seconds. Height (c) and stiffness (d) profiles along full line in image (a) and dashed line in image (b) are plotted with full and dashed lines respectively. Stiffness histograms related to AFM stiffness images in figure a (full line) and figure b (dots and dashed line) are presented in figure (e).

Figure 17

(a; b) : two successive AFM stiffness images of *Nostoc* are presented: scan size 20 μm x20 μm ; stiffness grey scale: 0.4N/m. Time interval is equal to 137 seconds. Height (c) and stiffness (d) profiles along full line in image (a) and dashed line in image (b) are plotted with full and dashed lines respectively.

Figure 18

Typical curves of force versus vertical piezo displacement (a_) and force versus indentation (b_) for *Nostoc* bacterium (_1), slime (_2) and ECM (_3) are plotted.

Figure 19

Typical curves of force versus vertical piezo displacement (a_) and force versus indentation (b_) for *Rhodococcus wratislaviensis* bacterium (_1) and slime (_2) are plotted.

Figure 20

Variation of the slime thickness versus the *Nostoc* gliding speed.

| | | | | Bacterium | | ECM | Slime | |
|---------------------------|-----------------|---------------------|-----------------|---------------------------|--------------------------|-----------------|-------------------------|----------------|
| Type of Bacterium | Sequence number | Gliding speed (m/s) | Figure numbers | Stiffness (N/m) | | Stiffness (N/m) | Stiffness (N/m) | Thickness (nm) |
| | | | | Mean value from histogram | Stiffest points | | | |
| <i>Nostoc</i> | #1 | 80 | 8; 9; 10; 11 | 0.09 / 0.12 | 0.18-0.22 / 0.36-0.57 | 0.07 / 0.09 | 0.26-0.30 / 0.94-1.8 | 5 |
| | #2 | 220 | 14; 15; | 0.18 / 0.36 | 0.23 / 0.64 | 0.16 / 0.29 | 0.21 / 0.50 | 20 |
| | #3 | 120 | 16; 17 | 0.07 / 0.09 | 0.2 / 0.45 | 0.03 / 0.04 | 0.21 / 0.50 | 8 |
| <i>R. wratislaviensis</i> | | 0 | 3; 4 | 0.23 / 0.64 | 0.24 / 0.72 | - | 0.12 / 0.18 | 250 |

Table 1

Values of effective stiffness and component stiffness (in italics) for the different studied bacteria and their different components.

| Type of Bacterium | Sequence number | Gliding speed (m/s) | Figure numbers | Turgor Pressure (kPa) |
|---------------------------|-----------------|---------------------|----------------|-----------------------|
| <i>Nostoc</i> | #1 | 80 | 8; 9; 10; 11 | 58 |
| | #2 | 220 | 14; 15; | 174 |
| | #3 | 120 | 16; 17 | 42 |
| <i>R. wratislaviensis</i> | | 0 | 3; 4 | 307 |

Table 2

Turgor pressure for the studied bacteria at different gliding speeds

| Type of Bacterium | | | Young modulus (MPa) |
|---------------------------|-----------|------------|------------------------|
| <i>Nostoc</i> | | | |
| <i>Nostoc</i> | Bacterium | Low speed | 20 ±3 |
| | | High speed | 63 ±5 |
| | ECM | Low speed | 4 ±2 |
| | | High speed | 15 ±3 |
| | Slime | Low speed | 1.1 ±1.0 |
| | | High speed | 20 ±3 |
| <i>R. wratislaviensis</i> | | | |
| <i>R. wratislaviensis</i> | Bacterium | | 104 ±5 |
| | Slime | | 4.3 ±.5 |

Table 3

Young modulus for the studied bacteria at different gliding speeds

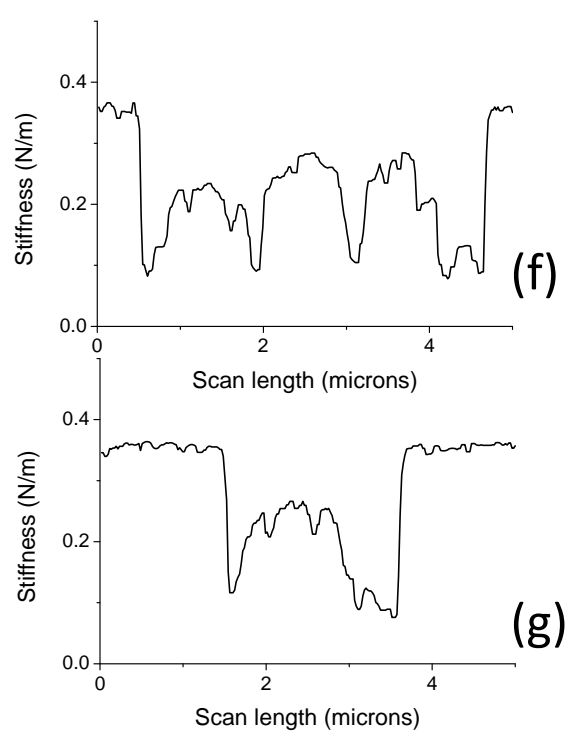
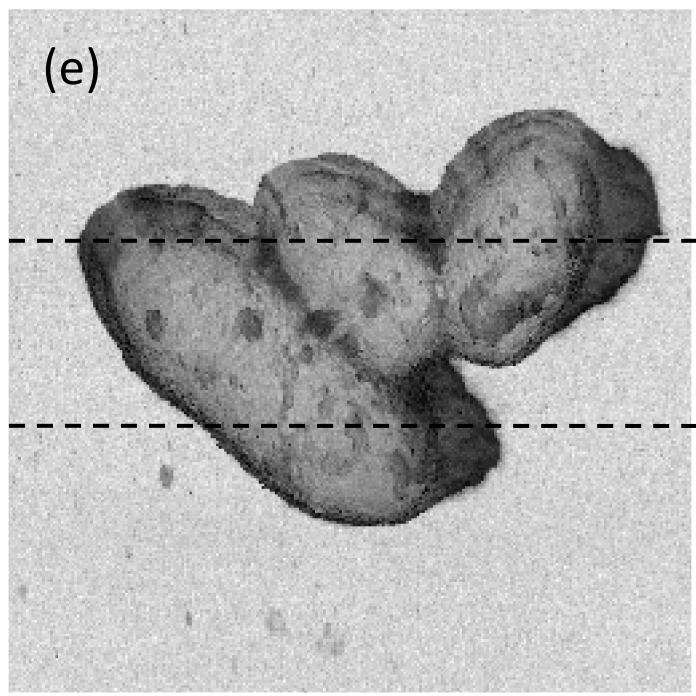
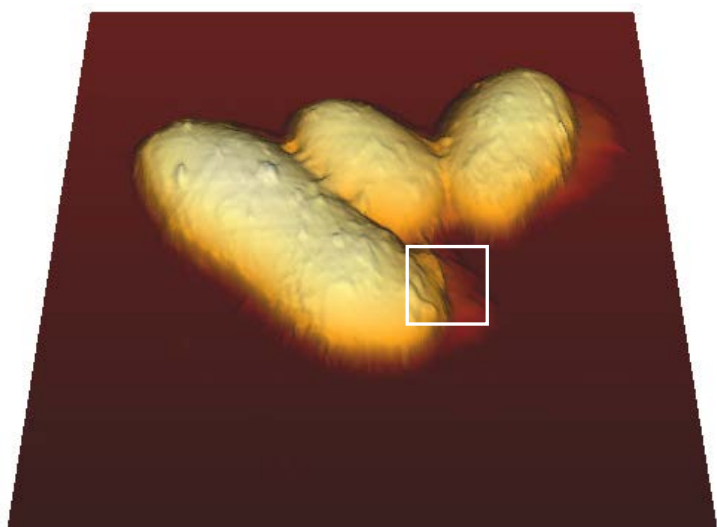
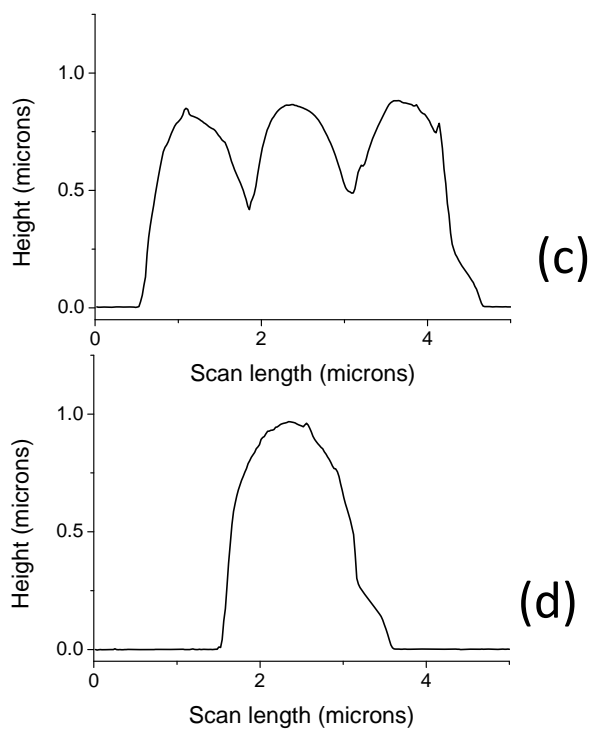
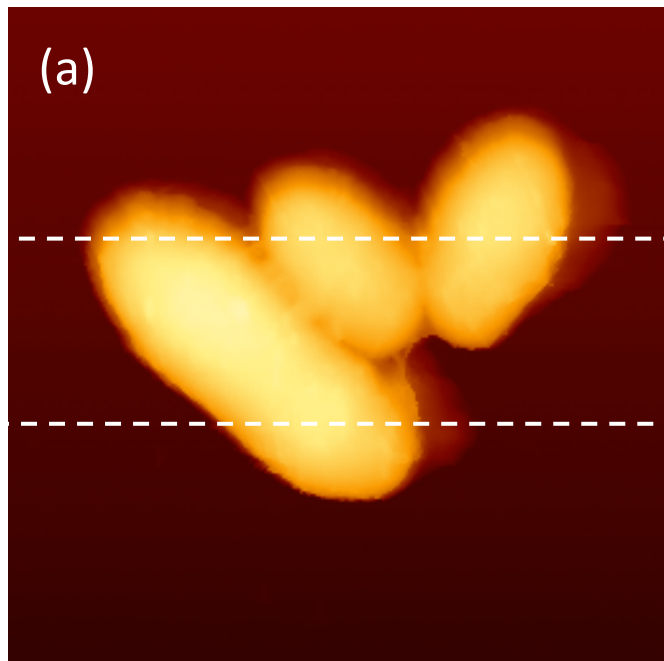


Figure 1

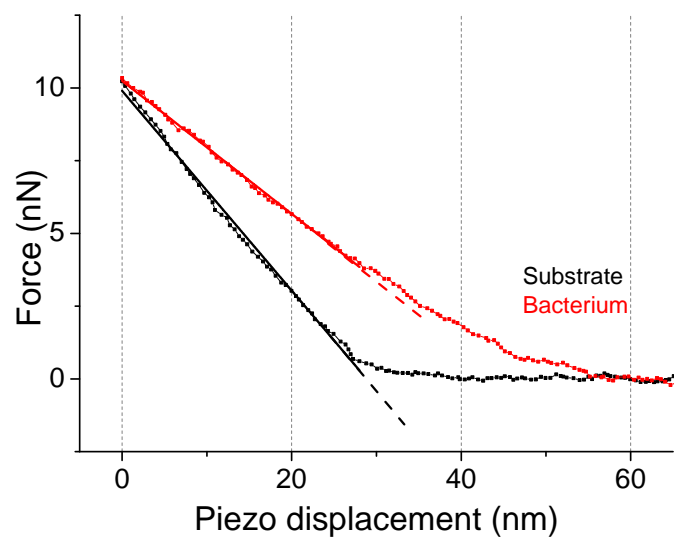


Figure 2

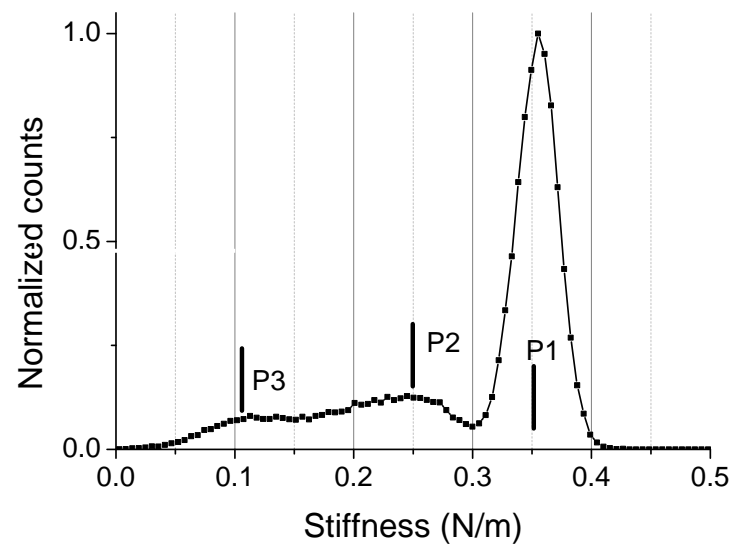


Figure 3

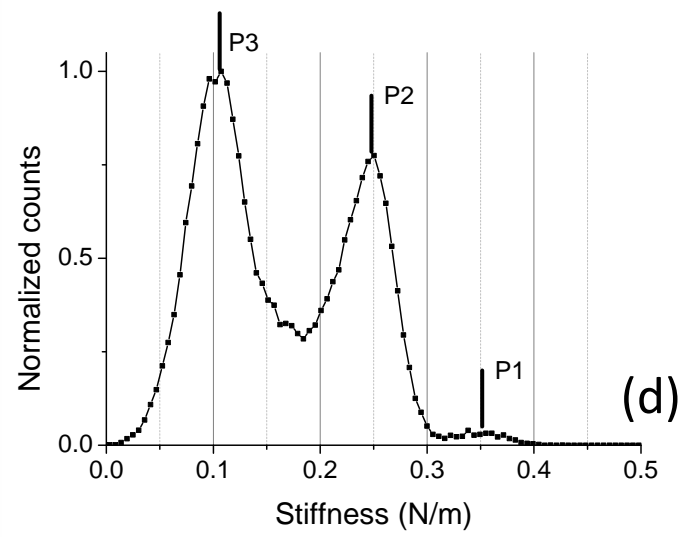
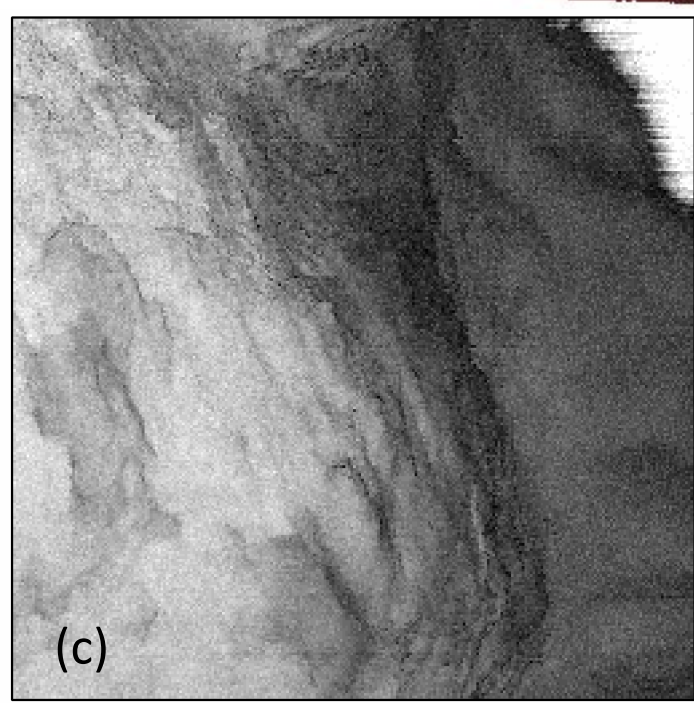
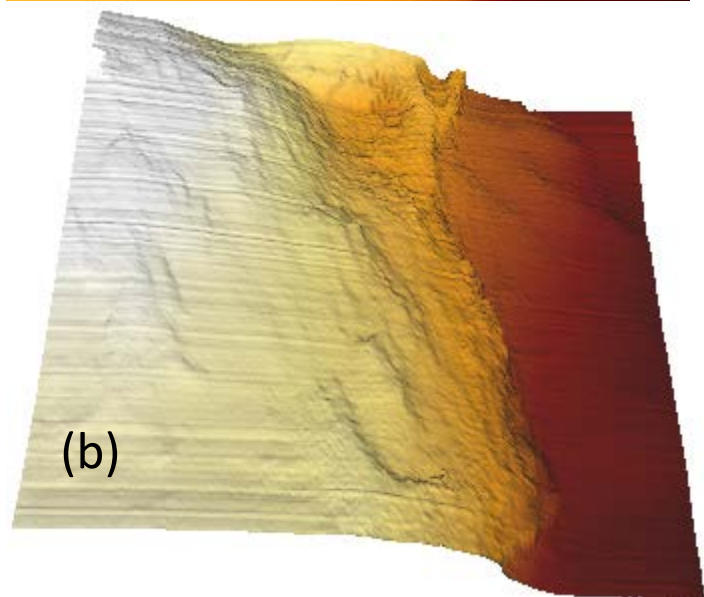
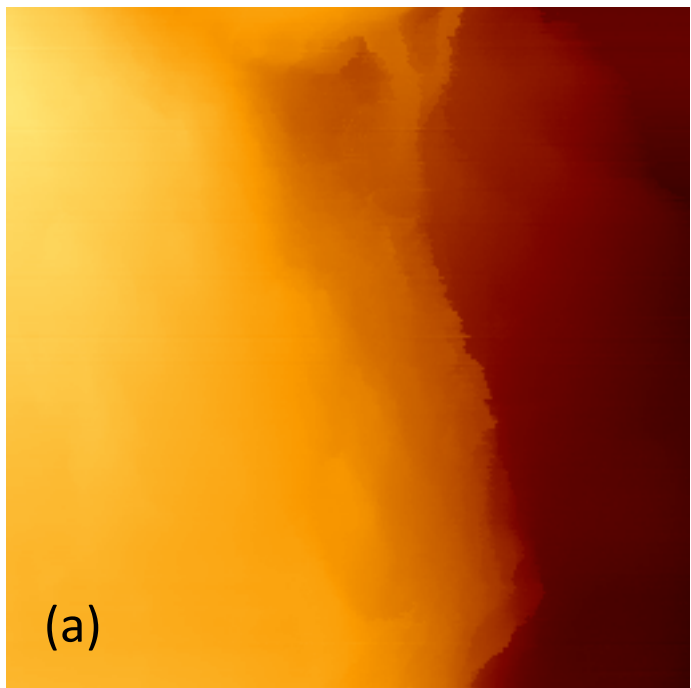


Figure 4

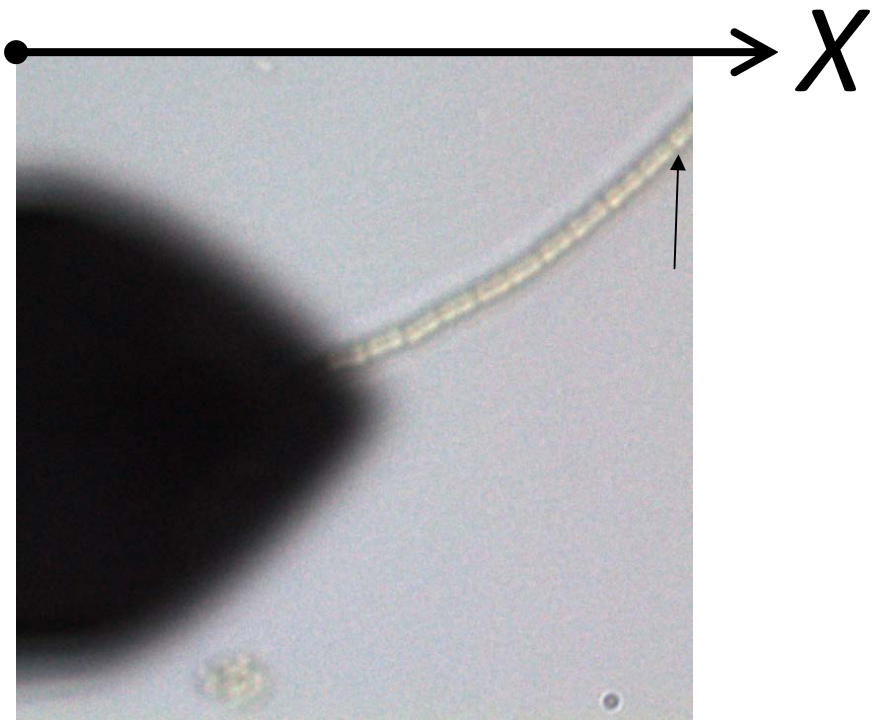
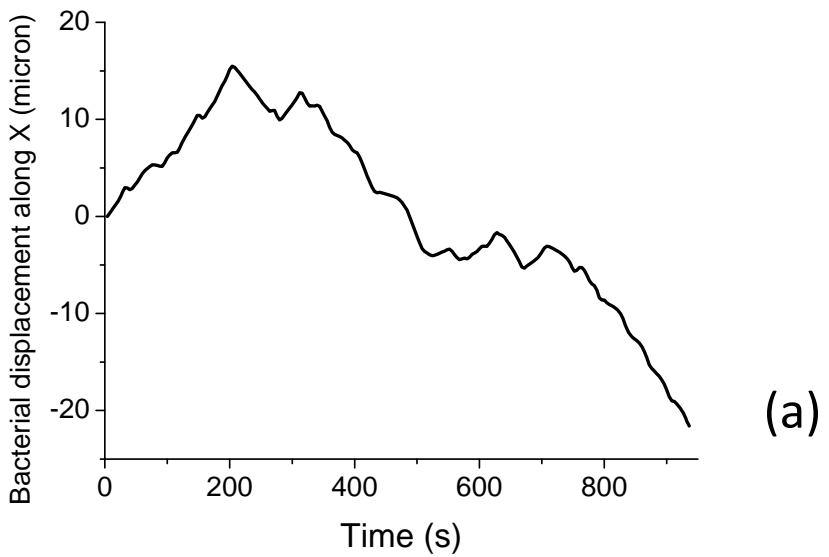
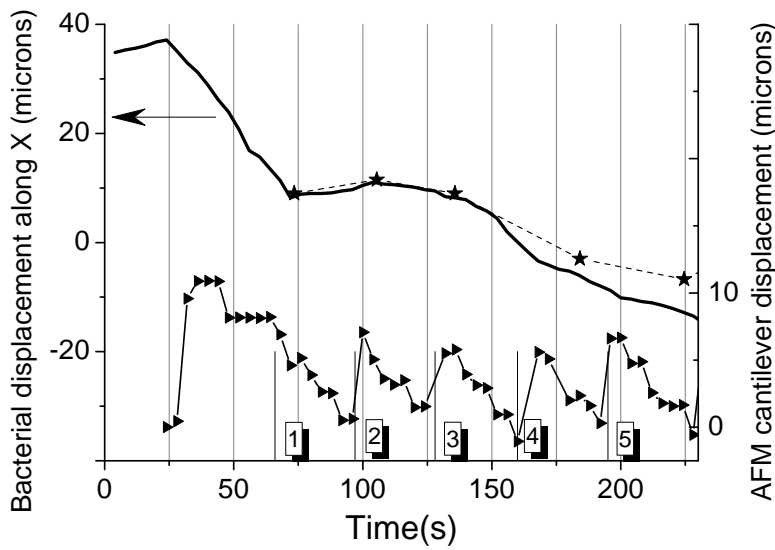


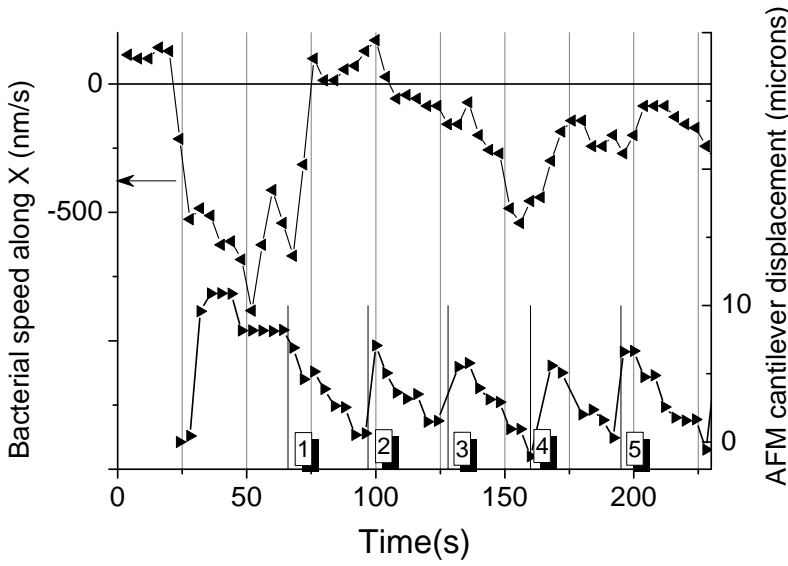
Figure 5



(a)



(b)



(c)

Figure 6

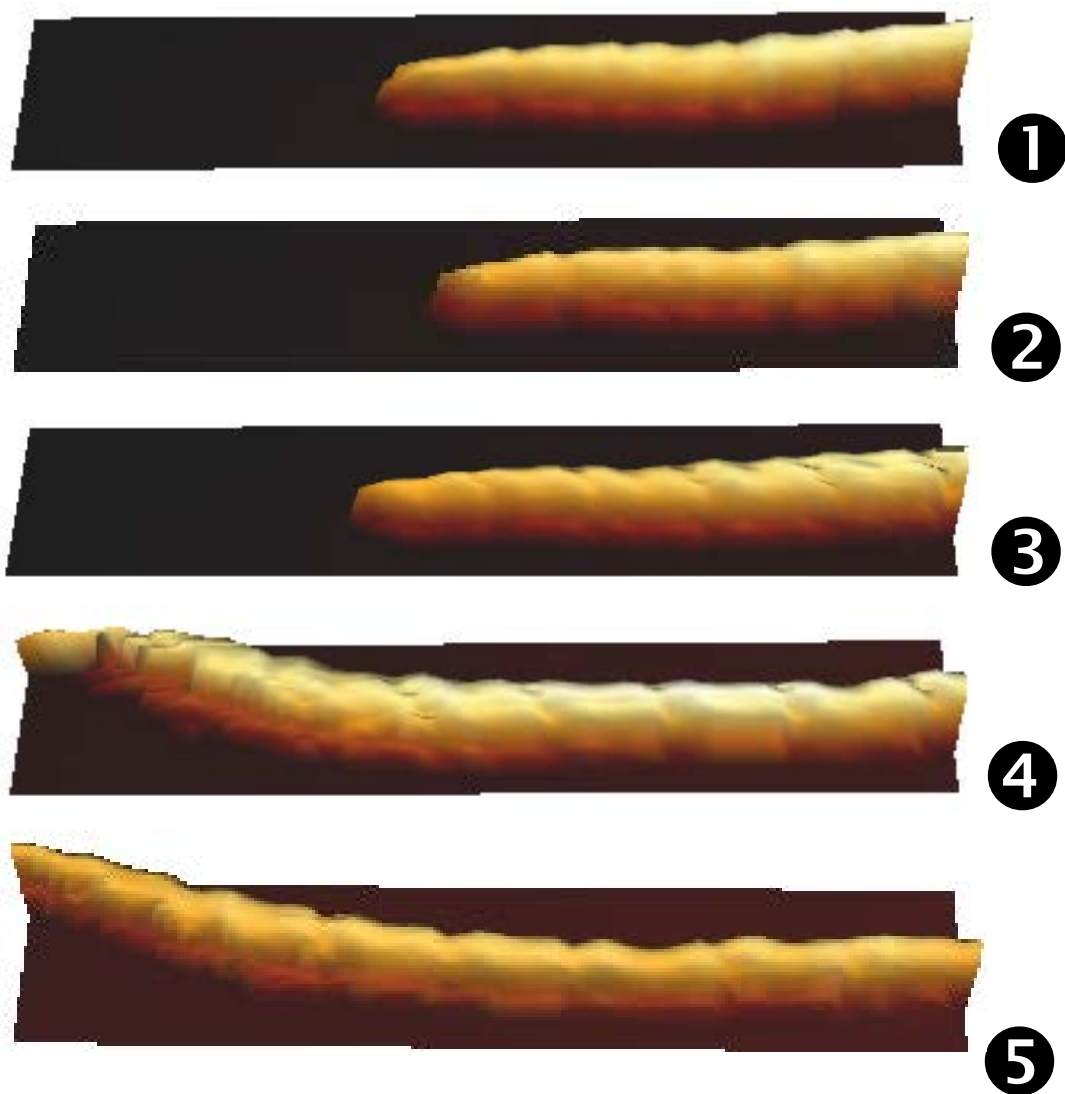


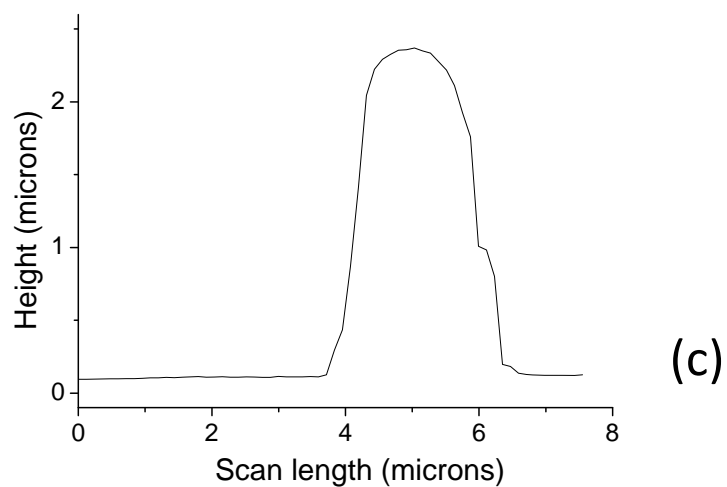
Figure 7



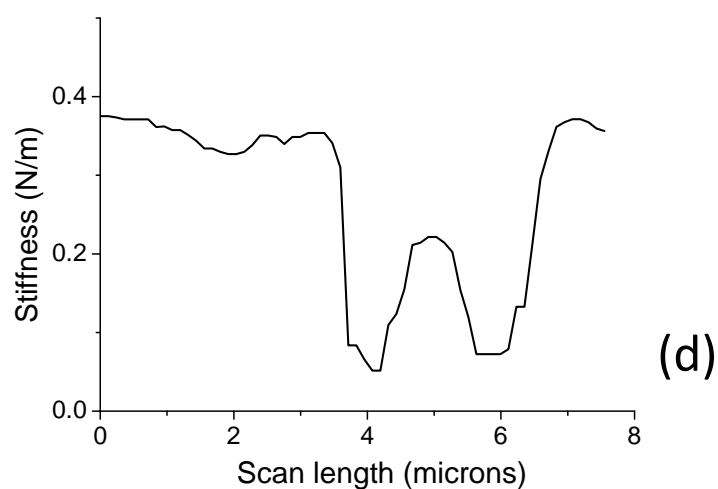
(a)



(b)



(c)



(d)

Figure 8

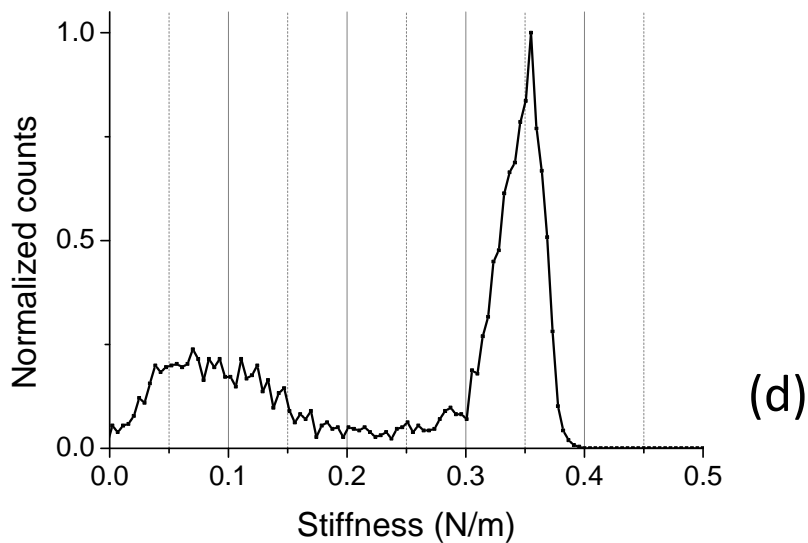
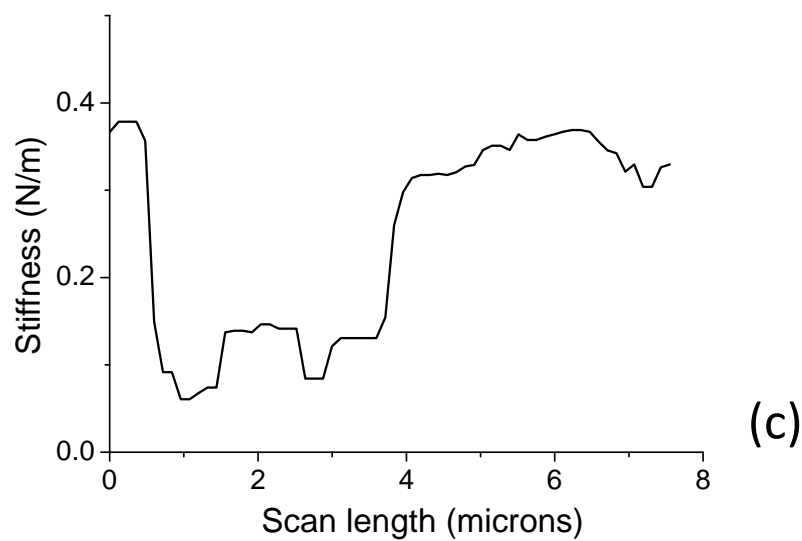
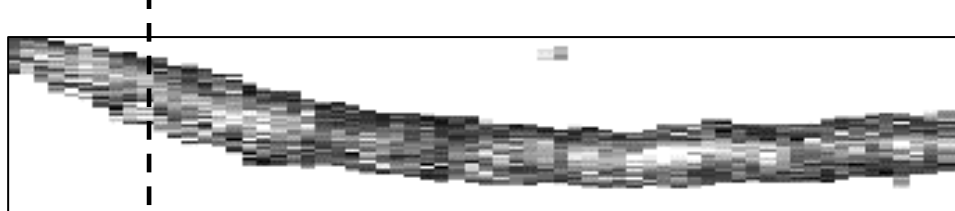


Figure 9

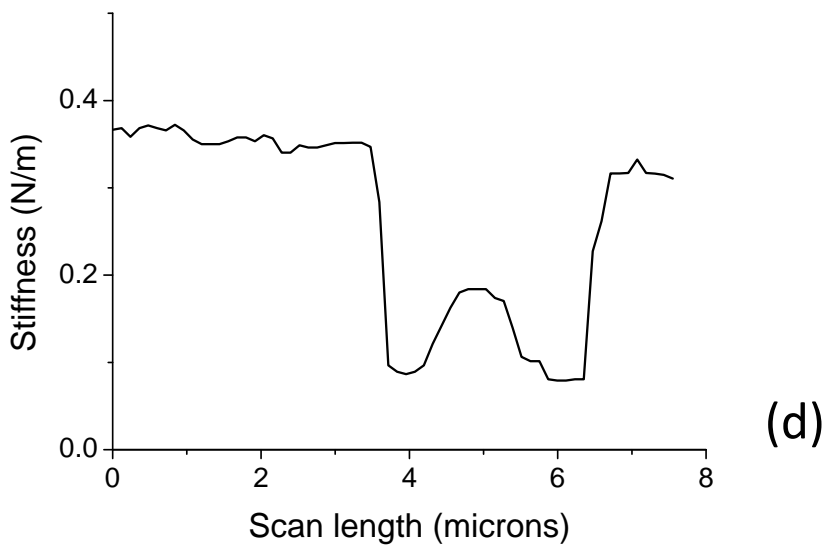
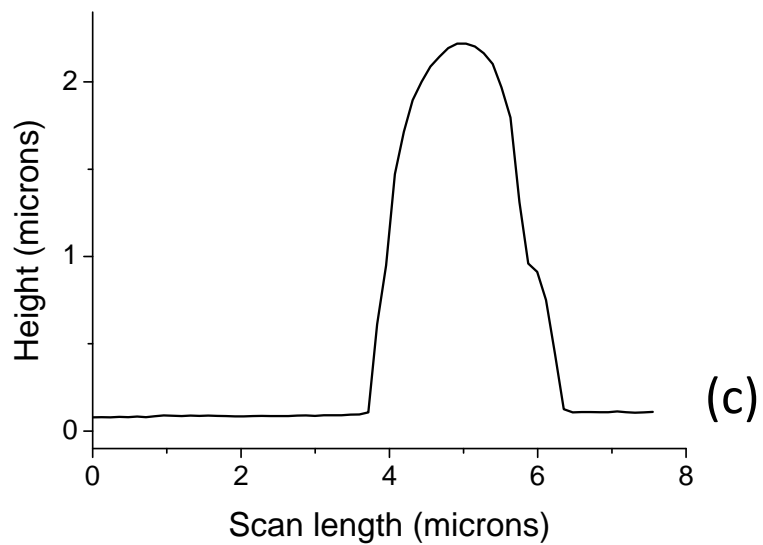
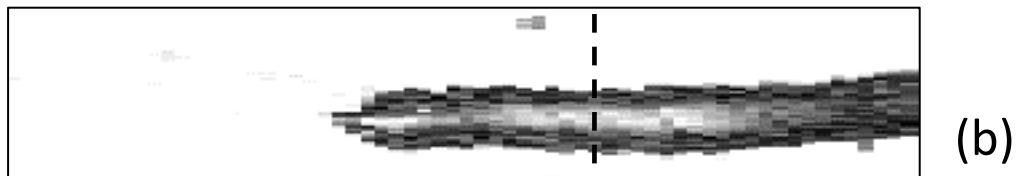
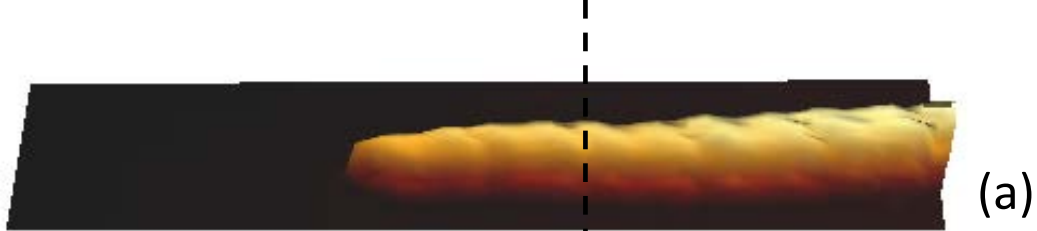


Figure 10

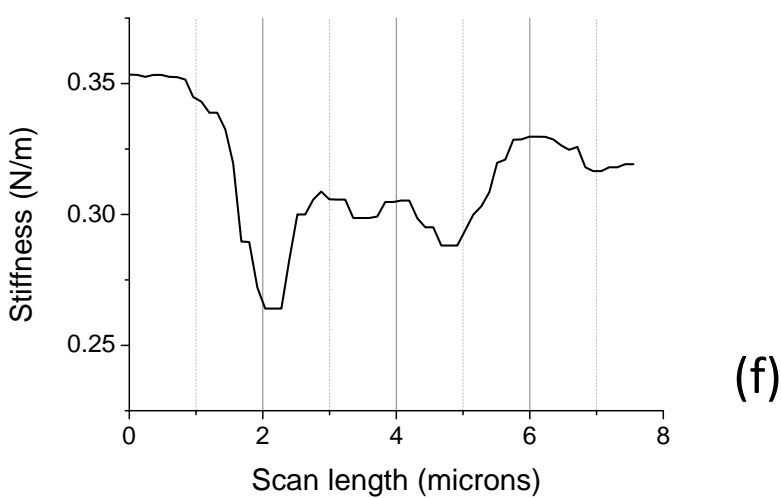
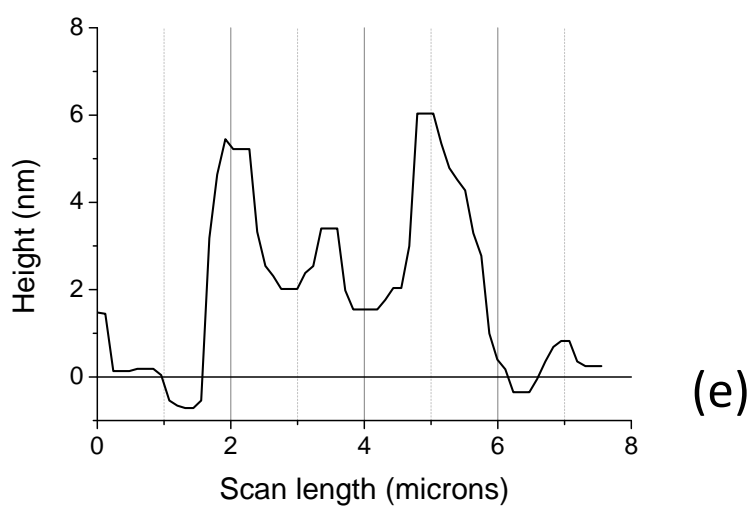
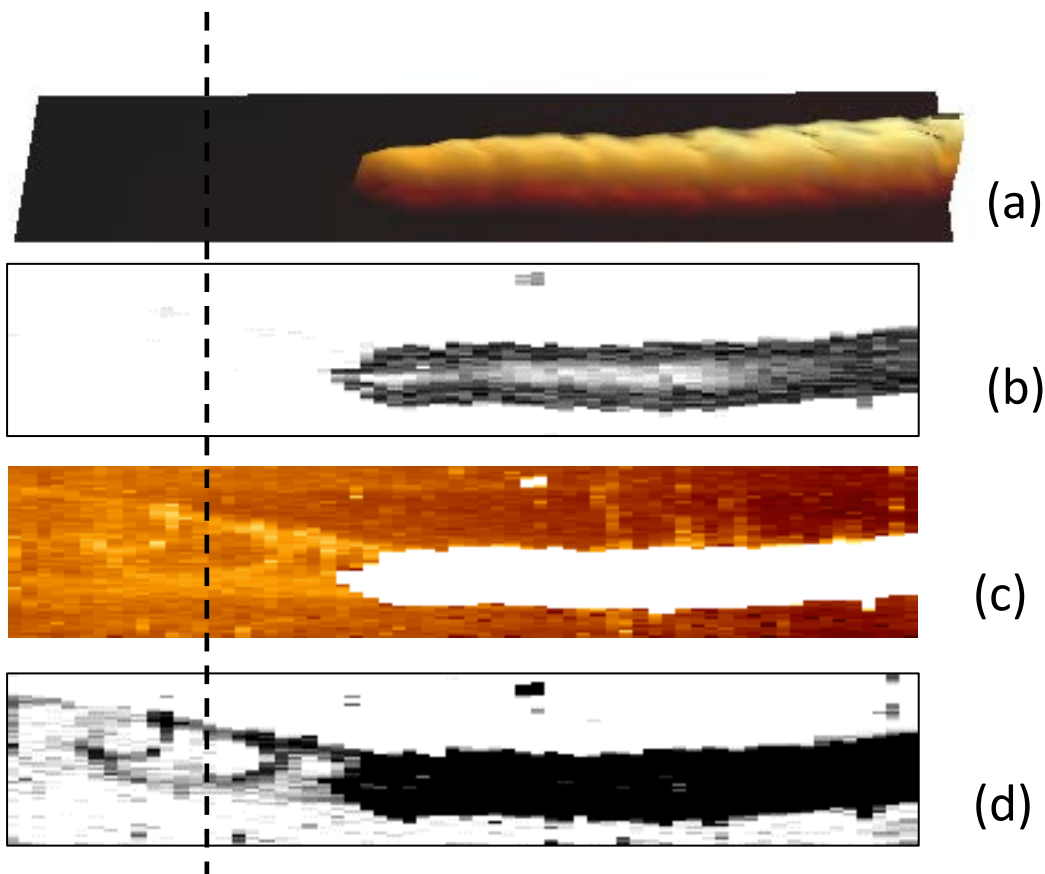


Figure 11

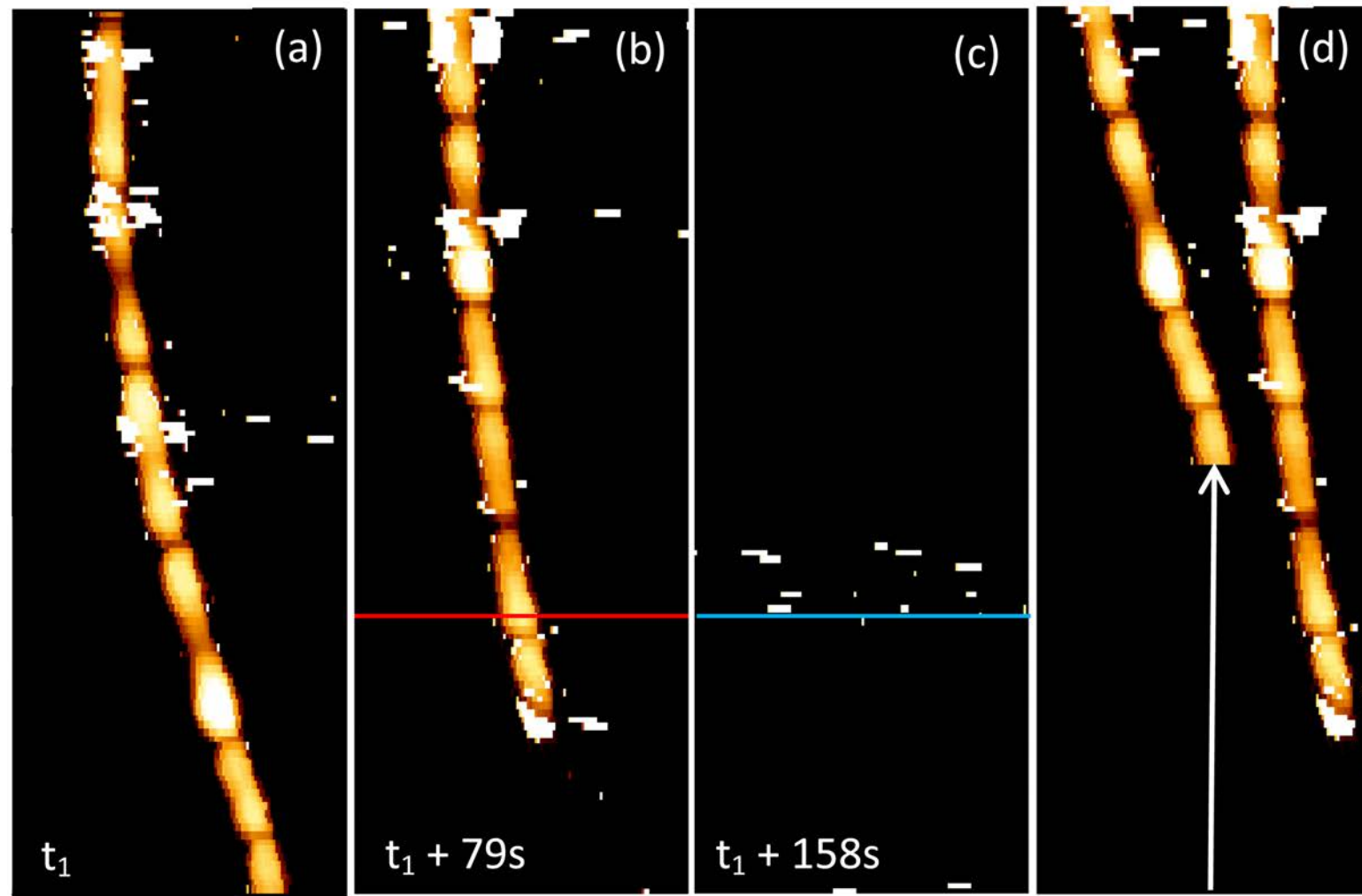


Figure 12

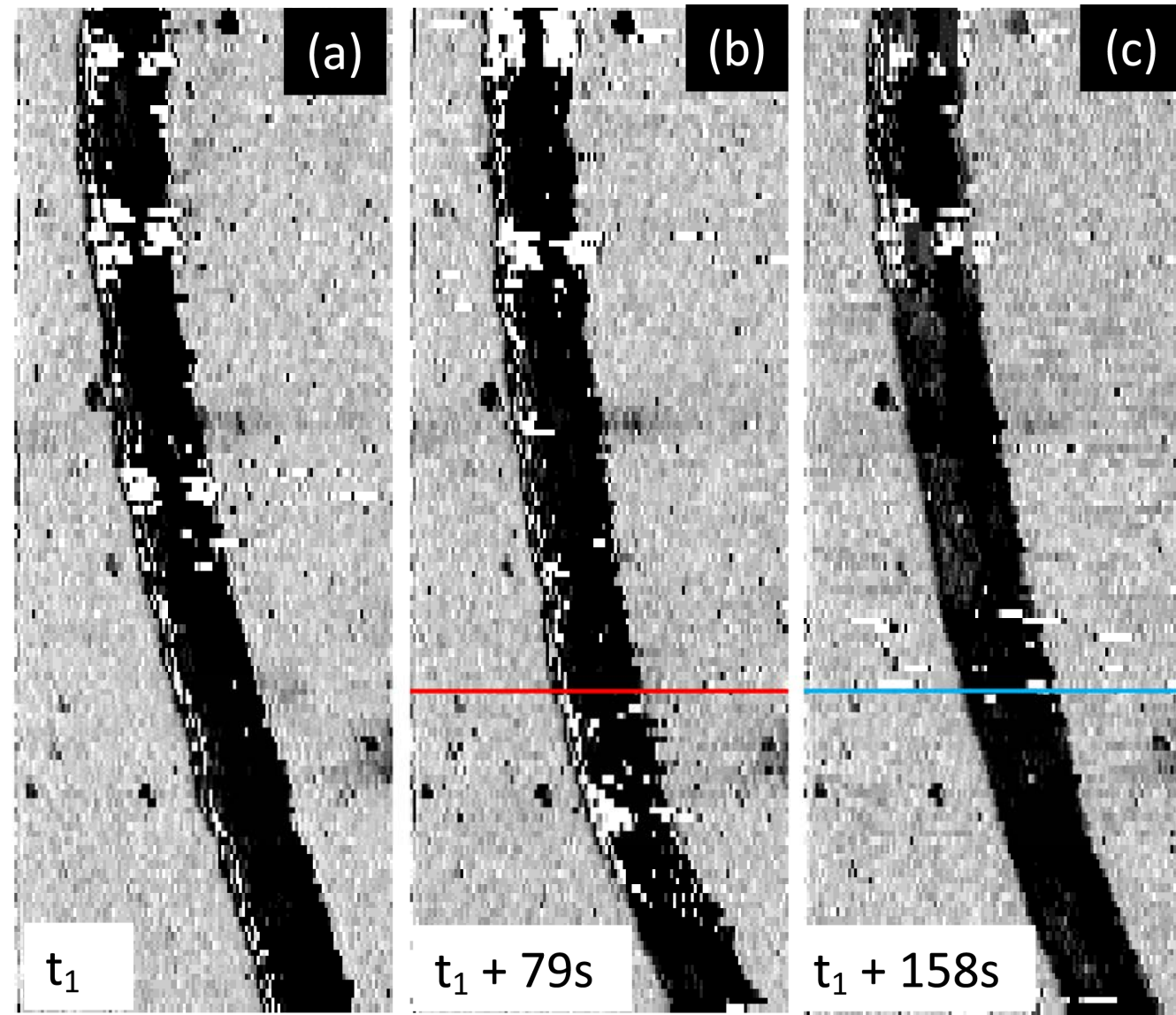


Figure 13

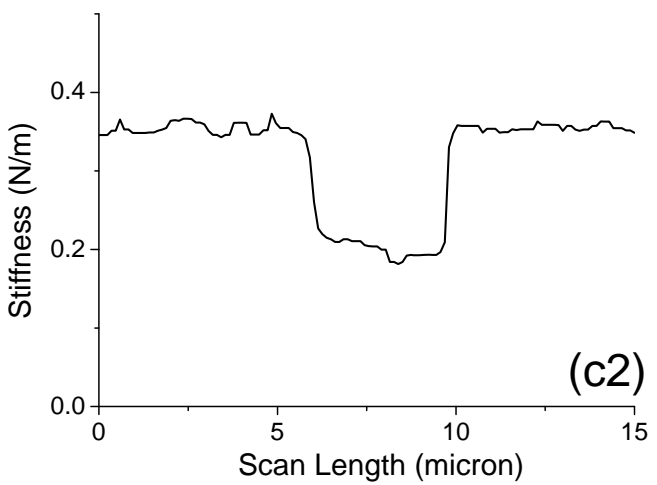
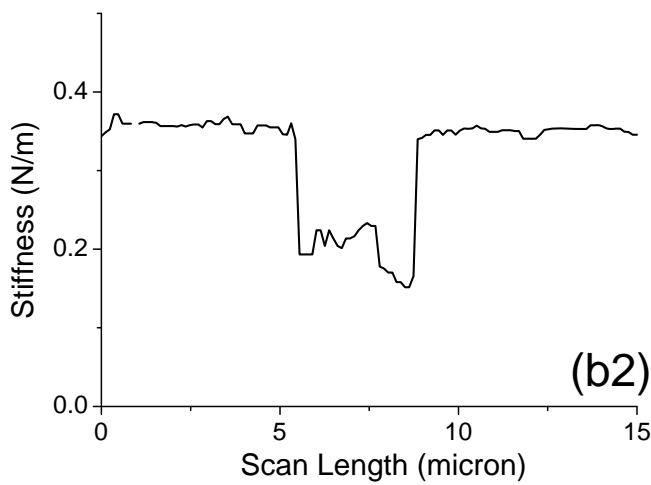
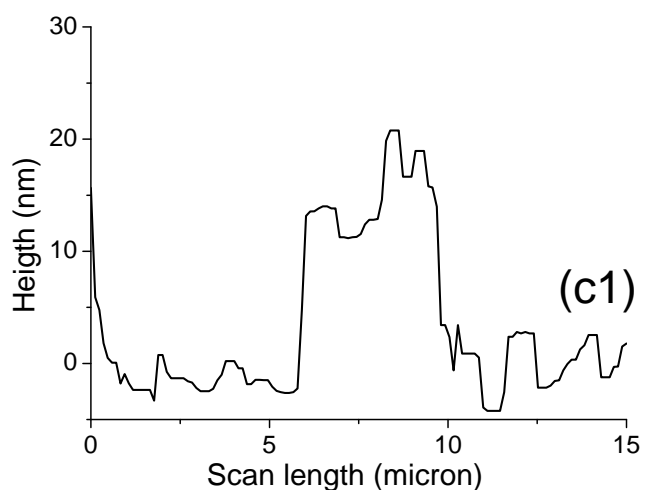
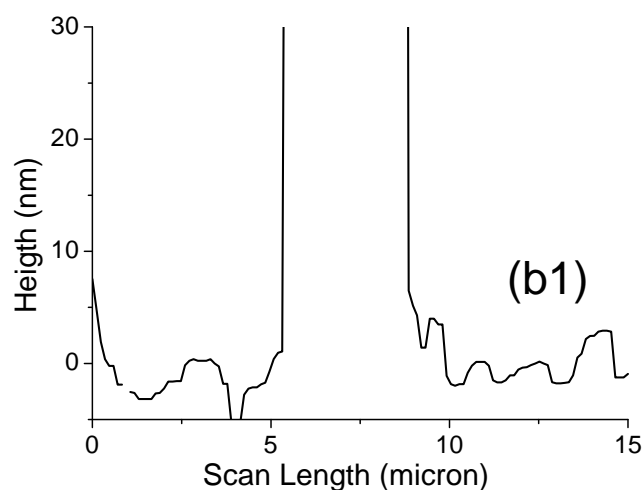
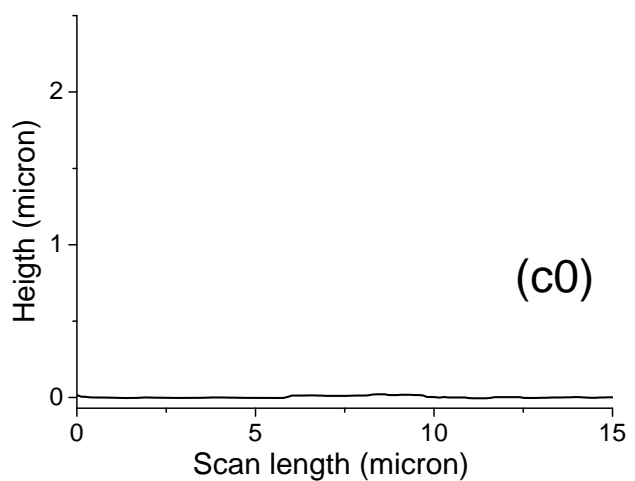
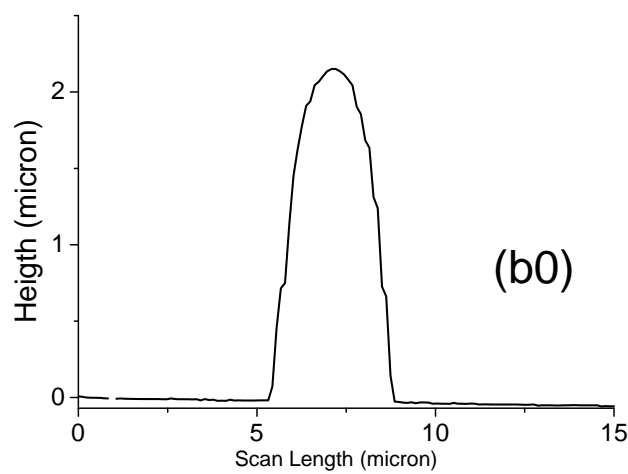


Figure 14

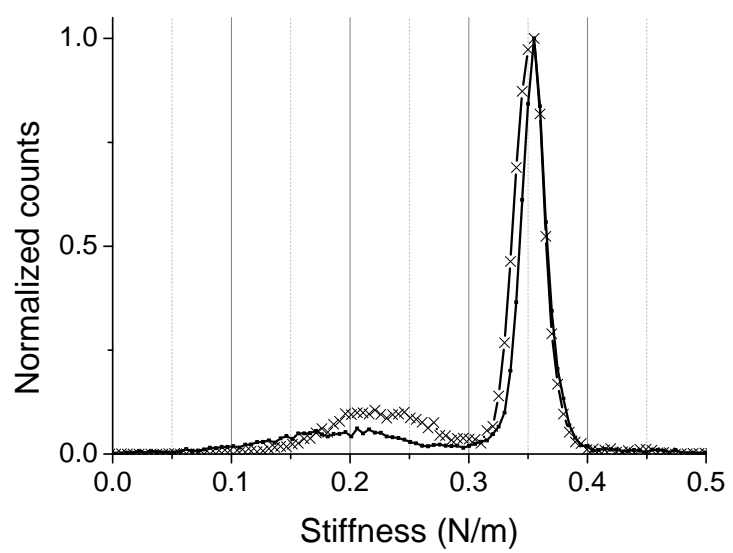


Figure 15

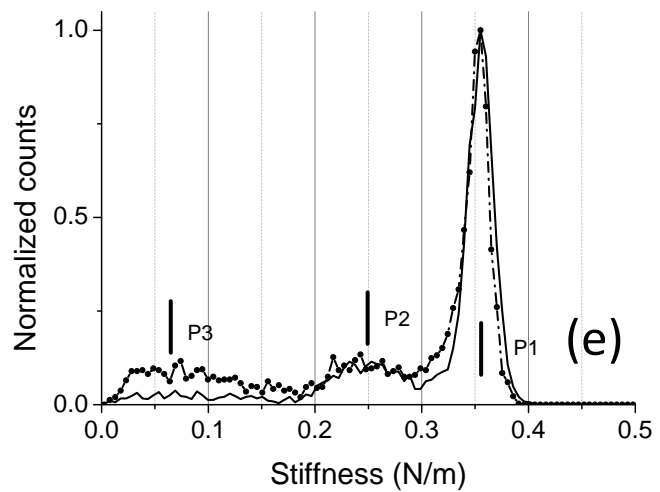
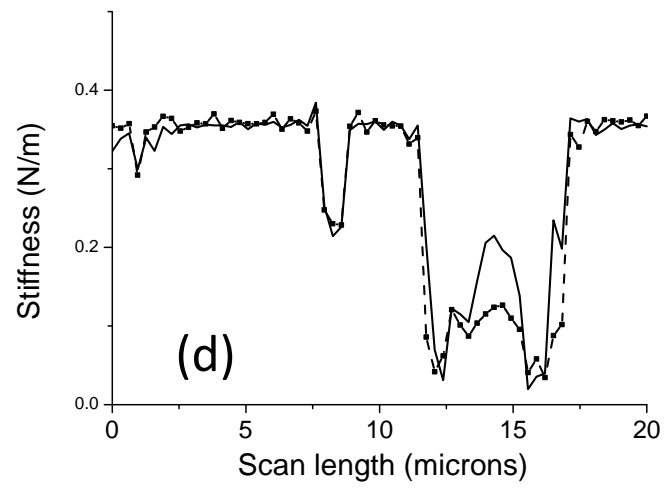
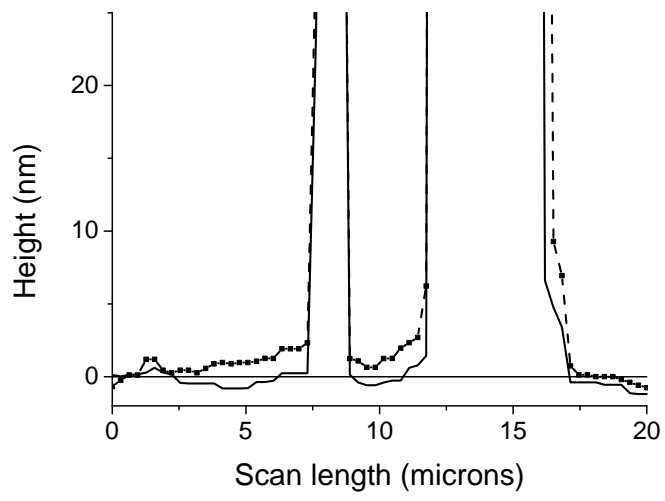
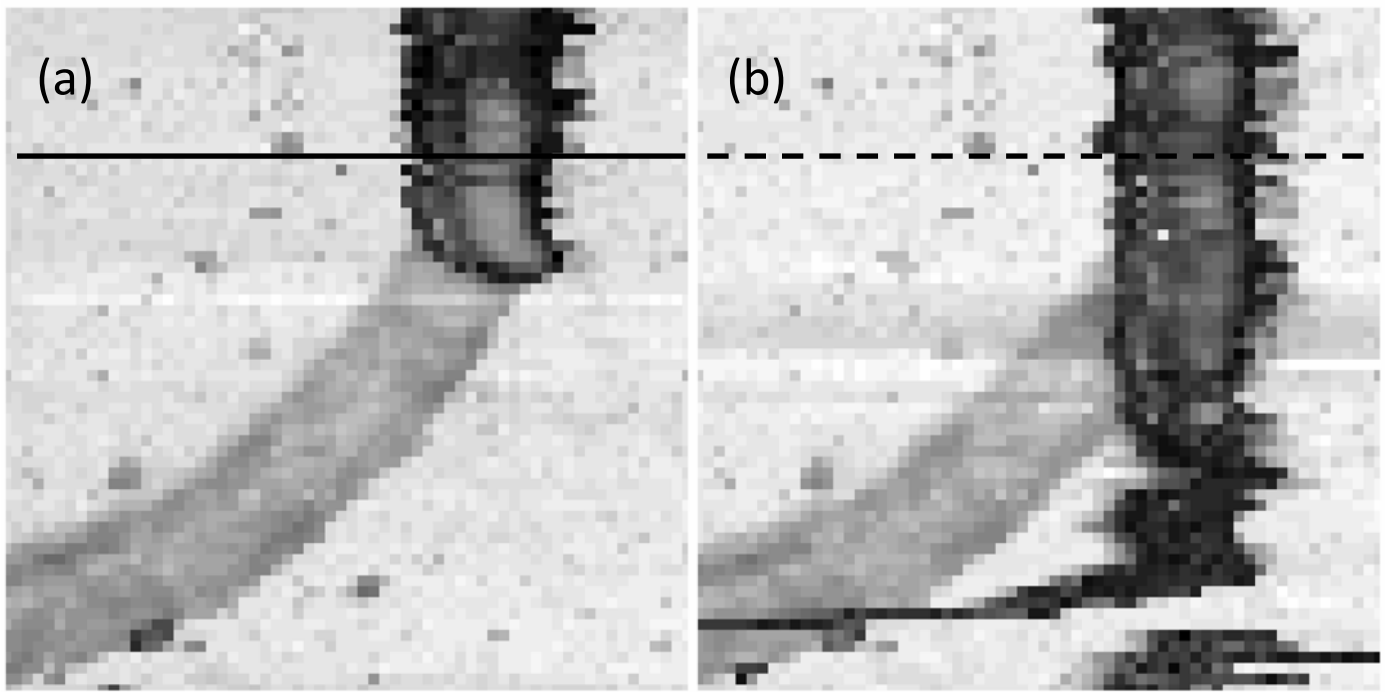


Figure 16

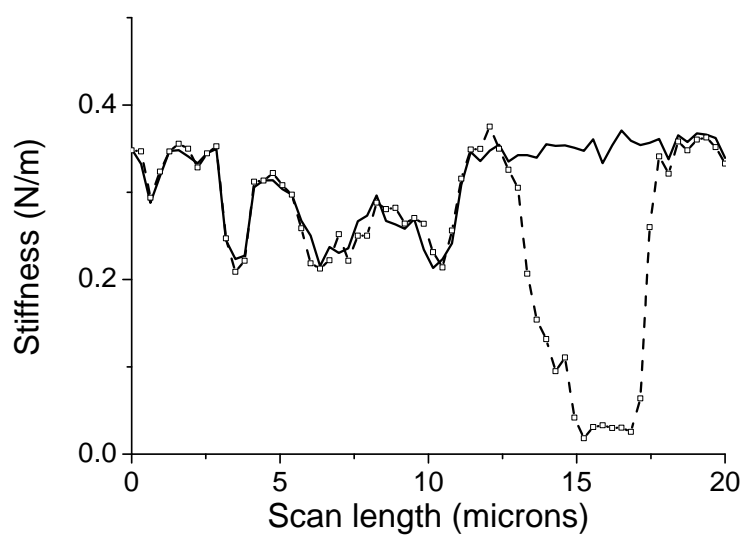
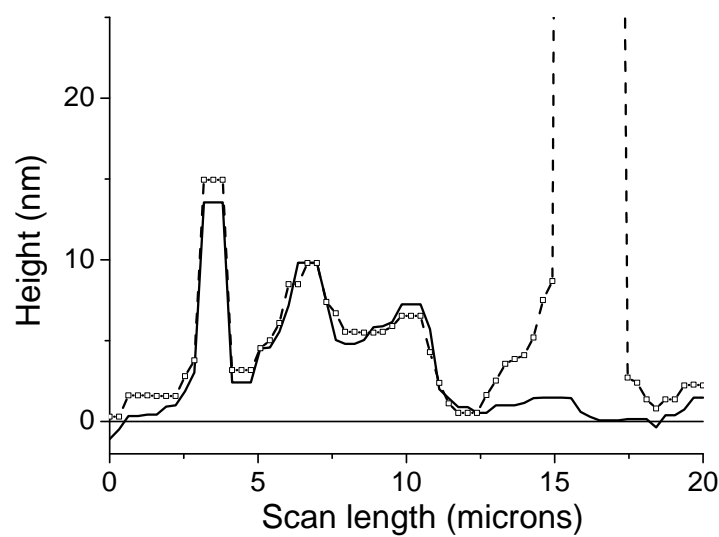
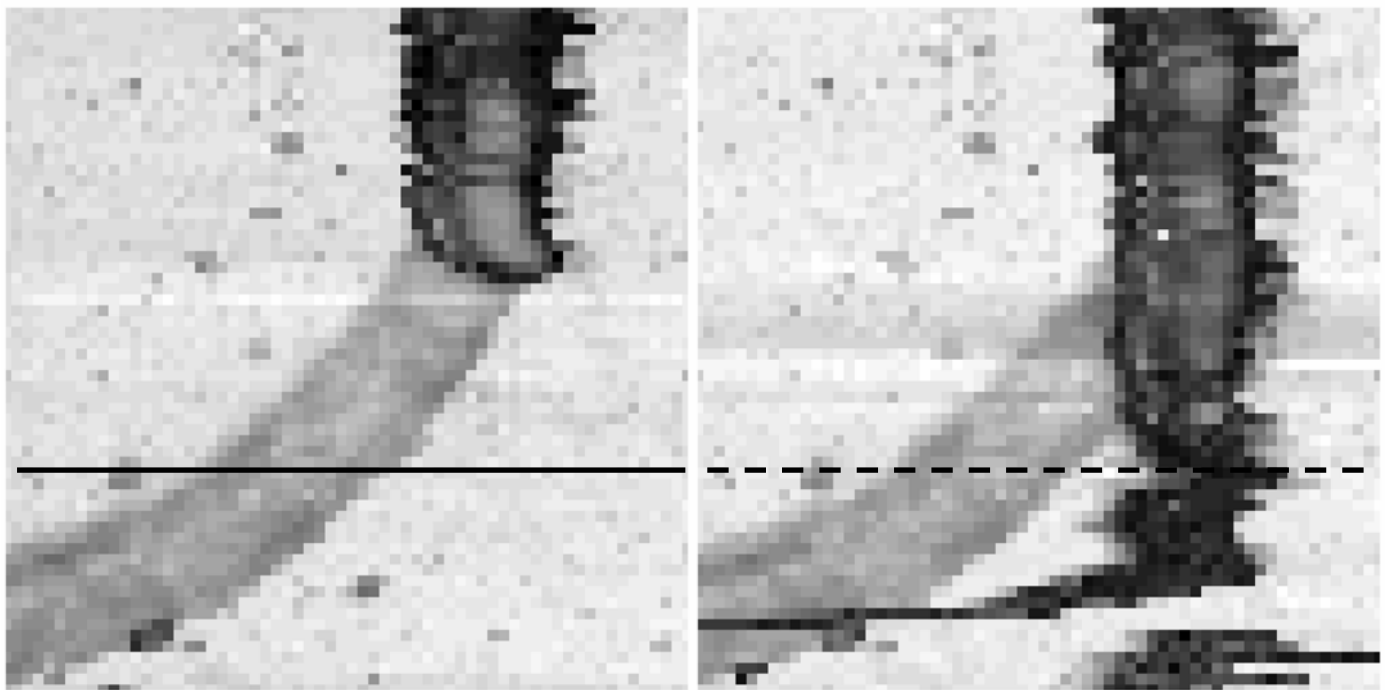


Figure 17

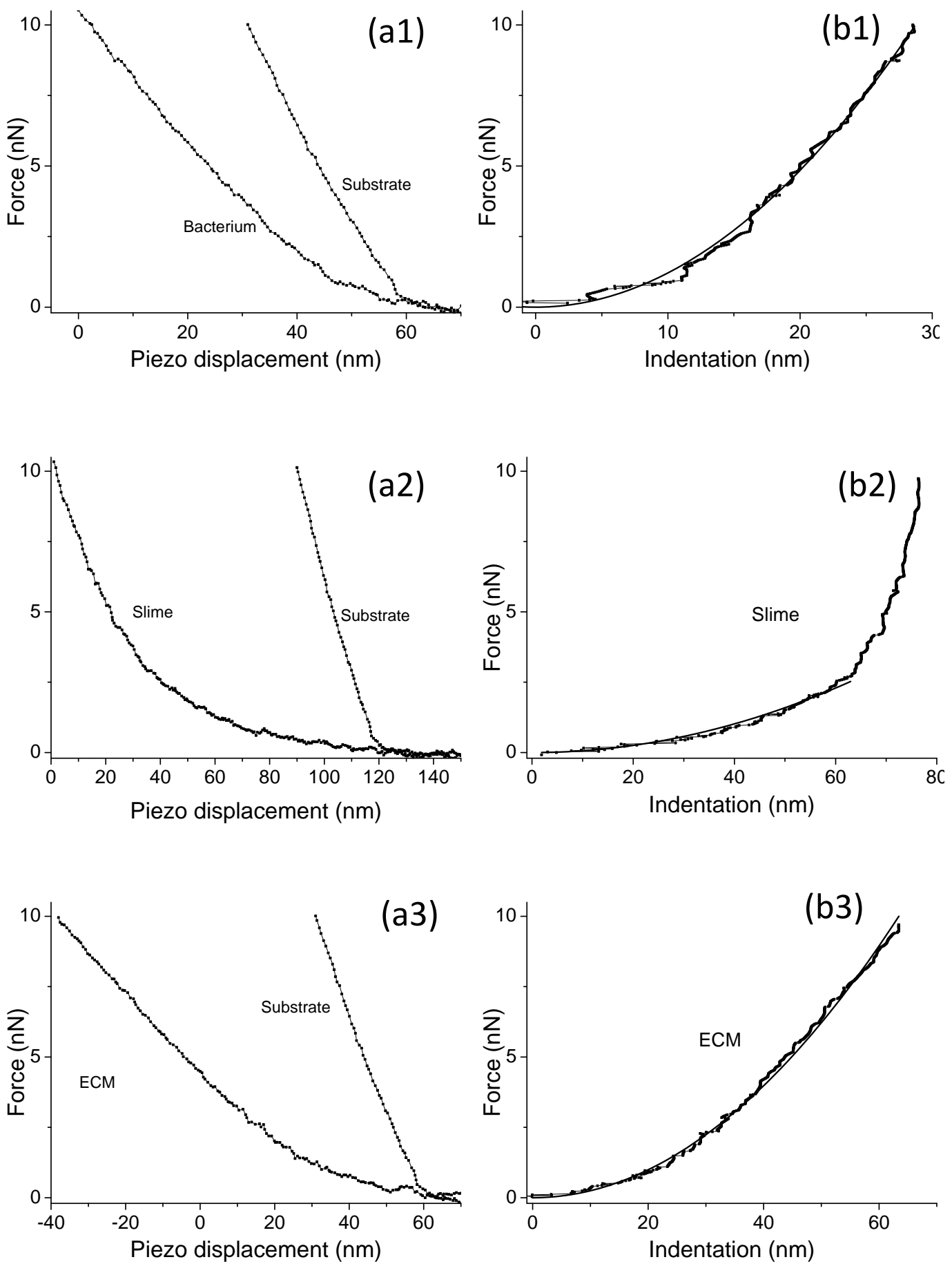


Figure 18

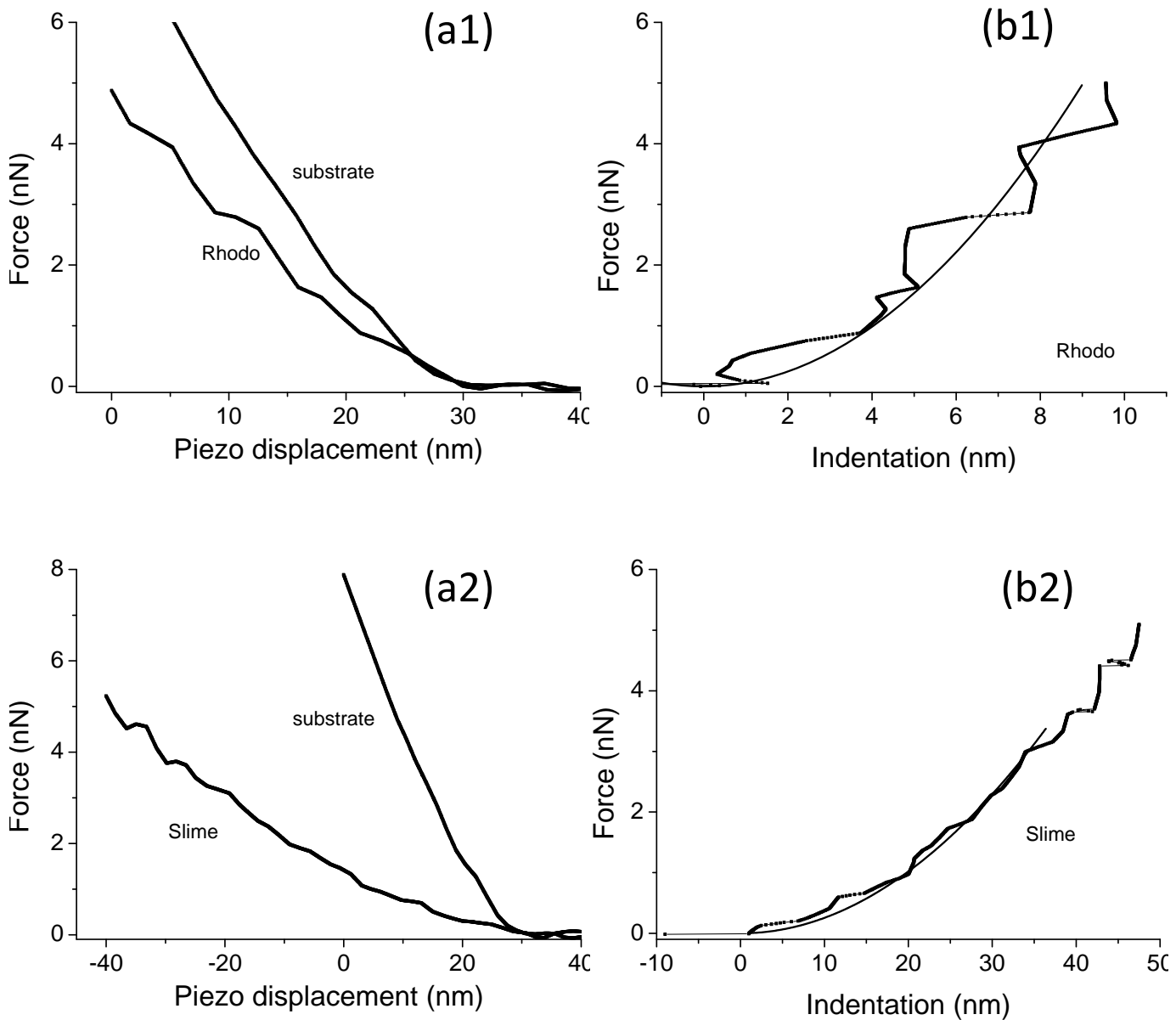


Figure 19

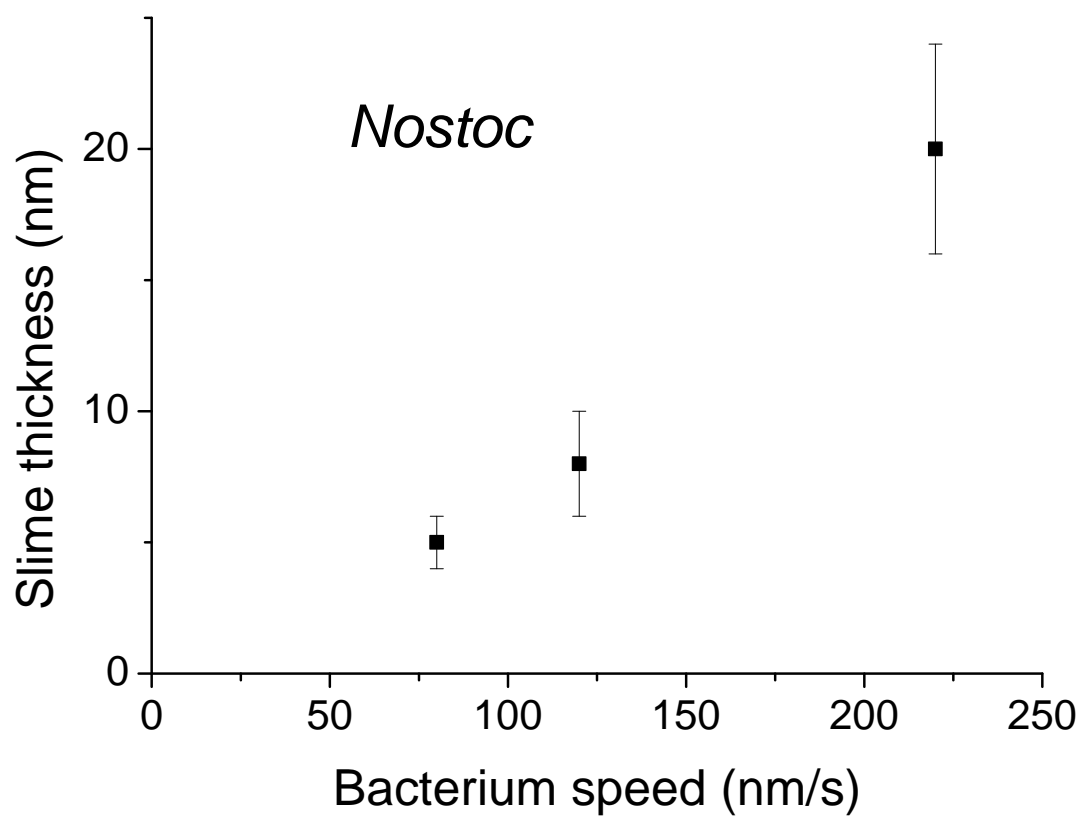


Figure 20